U.S. Department of Transportation

Federal Railroad Administration

Reference-Free Estimates of Railroad Bridge Displacement under Revenue Service Traffic

Office of Research,
Development
and Technology
Washington, DC 20590

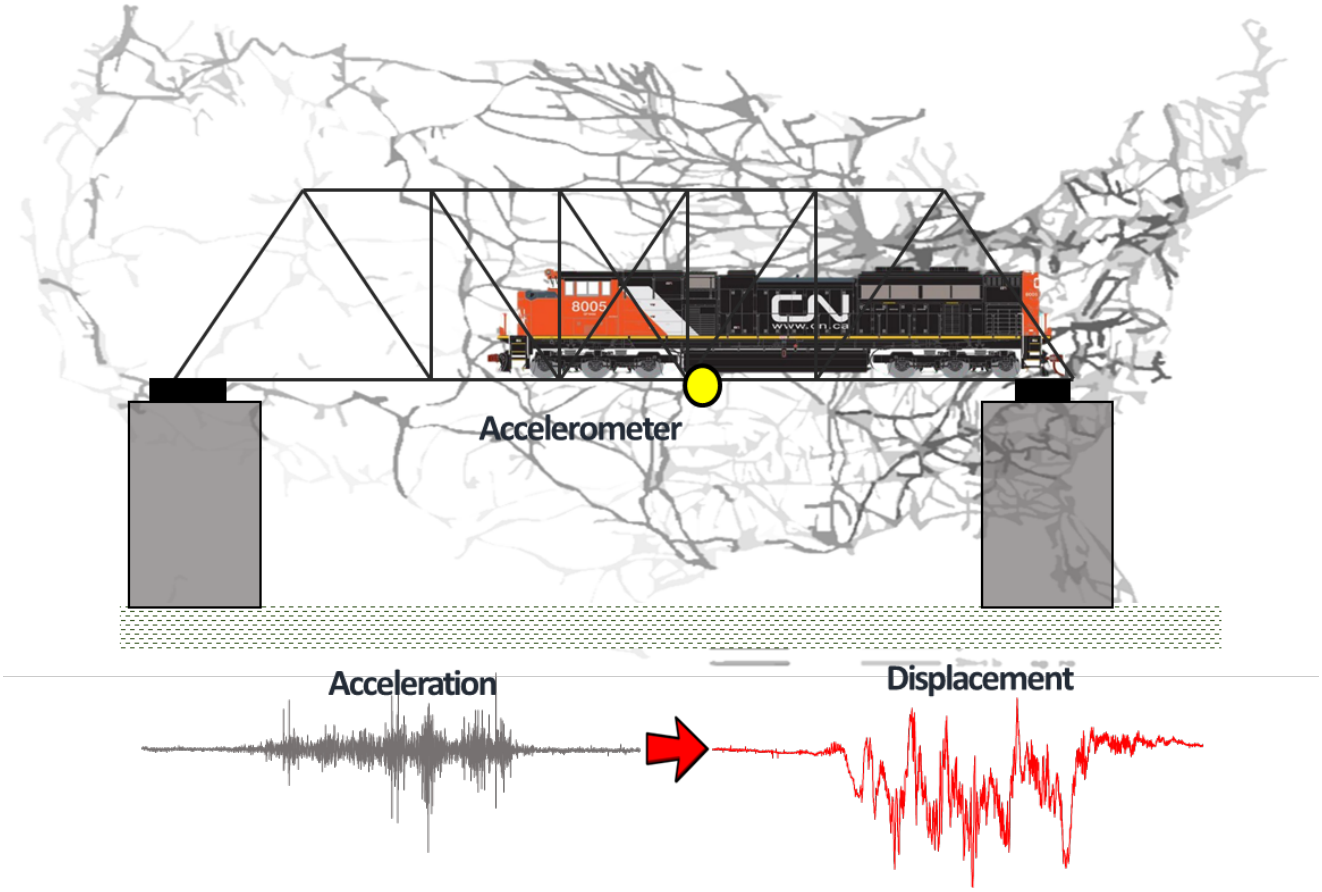

DOT/FRA/ORD-20/21

Final Report | May 2020

NOTICE

This document is disseminated under the sponsorship of the Department of Transportation in the interest of information exchange. The United States Government assumes no liability for its contents or use thereof. Any opinions, findings and conclusions, or recommendations expressed in this material do not necessarily reflect the views or policies of the United States Government, nor does mention of trade names, commercial products, or organizations imply endorsement by the United States Government. The United States Government assumes no liability for the content or use of the material contained in this document.

NOTICE

The United States Government does not endorse products or manufacturers. Trade or manufacturers' names appear herein solely because they are considered essential to the objective of this report.

REPORT DOCUMENTATION PAGE

Form Approved
OMB No. 0704-0188

Public reporting burden for this collection of information is estimated to average 1 hour per response, including the time for reviewing instructions, searching existing data sources, gathering and maintaining the data needed, and completing and reviewing the collection of information. Send comments regarding this burden estimate or any other aspect of this collection of information, including suggestions for reducing this burden, to Washington Headquarters Services, Directorate for Information Operations and Reports, 1215 Jefferson Davis Highway, Suite 1204, Arlington, VA 22202-4302, and to the Office of Management and Budget, Paperwork Reduction Project (0704-0188), Washington, DC 20503.

1. AGENCY USE ONLY (Leave blank)	2. REPORT DATE	3. REPORT TYPE AND DATES COVERED
	May 2020	Technical Report – May 2015 - August 2016

4. TITLE AND SUBTITLE
Reference-Free Estimates of Railroad Bridge Displacement under Revenue Service Traffic

5. FUNDING NUMBERS
DTFR53-15-C-00014

6. AUTHOR(S)
B.F. Spencer, F. Gomez, J. Park, H. Yoon, F. Moreu

7. PERFORMING ORGANIZATION NAME(S) AND ADDRESS(ES)
University of Illinois at Urbana-Champaign
Smart Structures Technology Laboratory
Department of Civil and Environmental Engineering
205 N. Matthews Ave.
Urbana, IL 61801

8. PERFORMING ORGANIZATION REPORT NUMBER

9. SPONSORING/MONITORING AGENCY NAME(S) AND ADDRESS(ES)
U.S. Department of Transportation
Federal Railroad Administration
Office of Railroad Policy and Development
Office of Research, Development and Technology
Washington, DC 20590

10. SPONSORING/MONITORING AGENCY REPORT NUMBER
DOT/FRA/ORD-20/21

11. SUPPLEMENTARY NOTES
COR: Cameron Stuart

12a. DISTRIBUTION/AVAILABILITY STATEMENT
This document is available to the public through the FRA eLibrary.

12b. DISTRIBUTION CODE

13. ABSTRACT (Maximum 200 words)
A top bridge research priority for railroad owners is to determine bridge displacements under in-service train loadings. Recent studies have demonstrated that displacement data assists railroad owners in prioritizing maintenance, repair, and replacement policies. However, displacement measurements are expensive to collect because of the need for static reference points. In this research project, UIUC has developed a straightforward and cost-effective means to estimate reference-free bridge displacements under in-service train loads from measured accelerations. The proposed system was validated for railroad bridges of higher interest/need of condition assessment by Class I railroads, such as timber trestles and steel trusses, with an emphasis in pin-connected trusses.

14. SUBJECT TERMS
Railroad bridge safety, bridge performance monitoring, reference-free displacements estimation, campaign monitoring

15. NUMBER OF PAGES
73

16. PRICE CODE

17. SECURITY CLASSIFICATION OF REPORT	18. SECURITY CLASSIFICATION OF THIS PAGE	19. SECURITY CLASSIFICATION OF ABSTRACT	20. LIMITATION OF ABSTRACT
Unclassified	Unclassified	Unclassified	

NSN 7540-01-280-5500
Standard Form 298 (Rev. 2-89)
Prescribed by ANSI Std. 239-18
298-102

METRIC/ENGLISH CONVERSION FACTORS

ENGLISH TO METRIC	METRIC TO ENGLISH
LENGTH (APPROXIMATE)	**LENGTH (APPROXIMATE)**
1 inch (in) = 2.5 centimeters (cm)	1 millimeter (mm) = 0.04 inch (in)
1 foot (ft) = 30 centimeters (cm)	1 centimeter (cm) = 0.4 inch (in)
1 yard (yd) = 0.9 meter (m)	1 meter (m) = 3.3 feet (ft)
1 mile (mi) = 1.6 kilometers (km)	1 meter (m) = 1.1 yards (yd)
	1 kilometer (km) = 0.6 mile (mi)
AREA (APPROXIMATE)	**AREA (APPROXIMATE)**
1 square inch (sq in, in^2) = 6.5 square centimeters (cm^2)	1 square centimeter (cm^2) = 0.16 square inch (sq in, in^2)
1 square foot (sq ft, ft^2) = 0.09 square meter (m^2)	1 square meter (m^2) = 1.2 square yards (sq yd, yd^2)
1 square yard (sq yd, yd^2) = 0.8 square meter (m^2)	1 square kilometer (km^2) = 0.4 square mile (sq mi, mi^2)
1 square mile (sq mi, mi^2) = 2.6 square kilometers (km^2)	10,000 square meters (m^2) = 1 hectare (ha) = 2.5 acres
1 acre = 0.4 hectare (he) = 4,000 square meters (m^2)	
MASS - WEIGHT (APPROXIMATE)	**MASS - WEIGHT (APPROXIMATE)**
1 ounce (oz) = 28 grams (gm)	1 gram (gm) = 0.036 ounce (oz)
1 pound (lb) = 0.45 kilogram (kg)	1 kilogram (kg) = 2.2 pounds (lb)
1 short ton = 2,000 pounds (lb) = 0.9 tonne (t)	1 tonne (t) = 1,000 kilograms (kg) = 1.1 short tons
VOLUME (APPROXIMATE)	**VOLUME (APPROXIMATE)**
1 teaspoon (tsp) = 5 milliliters (ml)	1 milliliter (ml) = 0.03 fluid ounce (fl oz)
1 tablespoon (tbsp) = 15 milliliters (ml)	1 liter (l) = 2.1 pints (pt)
1 fluid ounce (fl oz) = 30 milliliters (ml)	1 liter (l) = 1.06 quarts (qt)
1 cup (c) = 0.24 liter (l)	1 liter (l) = 0.26 gallon (gal)
1 pint (pt) = 0.47 liter (l)	
1 quart (qt) = 0.96 liter (l)	
1 gallon (gal) = 3.8 liters (l)	
1 cubic foot (cu ft, ft^3) = 0.03 cubic meter (m^3)	1 cubic meter (m^3) = 36 cubic feet (cu ft, ft^3)
1 cubic yard (cu yd, yd^3) = 0.76 cubic meter (m^3)	1 cubic meter (m^3) = 1.3 cubic yards (cu yd, yd^3)
TEMPERATURE (EXACT)	**TEMPERATURE (EXACT)**
[(x-32)(5/9)] °F = y °C	[(9/5) y + 32] °C = x °F

QUICK INCH - CENTIMETER LENGTH CONVERSION

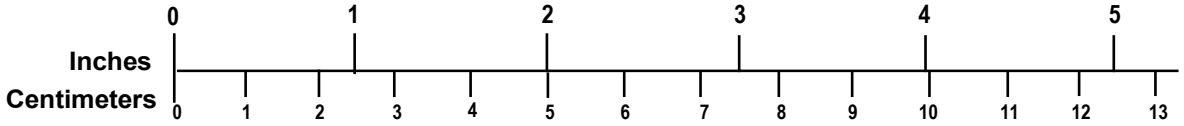

QUICK FAHRENHEIT - CELSIUS TEMPERATURE CONVERSIO

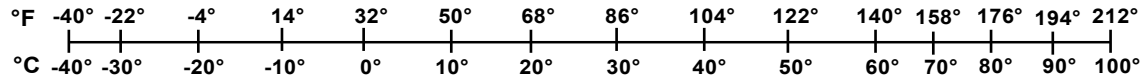

For more exact and or other conversion factors, see NIST Miscellaneous Publication 286, Units of Weights and Measures. Price $2.50 SD Catalog No. C13 10286

Updated 6/17/98

Acknowledgements

The Smart Structures Technology Laboratory and the Rail Transportation and Engineering Center thank Canadian National Railway (CN) for providing access to railroad bridge sites and for their technical support of this research. In particular, the authors thank the following CN personnel: Sandro Scola (Assistant Chief Bridge Engineer, Bridge Structures) for general coordination and James Tuchscherer (Bridge Inspector) for their bridge access and coordination support.

Contents

Illustrations

Tables

Executive Summary

A top research priority of the railroad bridge structural engineering community in North America is to develop a method to measure bridge displacements under revenue service traffic. Lateral and vertical displacements of bridges under trainloads are widely believed to provide a good measure of the condition of a bridge, and recent studies have demonstrated that such displacements can assist railroads in prioritizing maintenance, repair, and replacement policies. However, displacements are difficult to measure due to limited access and the need for fixed reference points. Furthermore, displacement performance limits for railroad bridges are not available in the current literature, and most of the specified limits are only suitable for design analysis. Therefore, researchers began this project by summarizing current concerns of the railroad industry regarding displacements of bridges under revenue service trains.

University of Illinois researchers developed new method based on a variational formulation that can accurately determine dynamic displacements from measured accelerations. This algorithm employs a digital filtering approach that is well-suited for implementation on wireless smart sensors. Researchers validated this algorithm numerically and experimentally in the laboratory as well as through field tests.

The output of this research project provides a means to estimate reference-free dynamic bridge displacements under in-service train loads and has applications in both campaign monitoring and the long-term or permanent monitoring of railroad bridges. Researchers confirmed the efficacy of the proposed system through tests of three Canadian National Railway railroad bridges in Illinois.

Successful completion of this research project provides a strong foundation for using estimated bridge displacements to develop bridge performance and safety thresholds that can assist railroads in managing and maintaining bridge assets and prioritizing repairs.

1. Introduction

This report documents the laboratory and field activities associated with developing and testing a novel wireless railroad bridge displacement estimation system. This project was conducted by University of Illinois at Urbana-Champaign researchers under contract with the Federal Railroad Administration's Office of Research, Development and Technology. The period of performance of this project was May 2015 to August 2016. All work was performed at university and Canadian National Railway locations.

1.1 Background

A 2012 survey of North American railroad bridge structural engineers[1] determined that a top bridge research priority is to develop a means for quantifying bridge displacements under revenue service train loads. The survey indicated that railroads are interested in methods to collect bridge displacements during their inspections. Moreu et al.[2] identified that bridge condition decay correlates highly with increasing transverse displacements in timber trestle bridges, and they provided preliminary recommendations for using transverse displacements as one measure to prioritize bridge inspection, maintenance, and replacement policies. However, two significant problems hinder the use of displacements in bridge condition assessment:

1) Displacements are difficult and expensive to measure due to the need for fixed references. The scarcity of displacement measurements of railroad bridges to date has been due, in part, to the high cost of instrumenting a railroad bridge to measure displacements under revenue service traffic. Figure 1.1 shows a typical field setup to measure displacements. In many circumstances, installing a fixed reference sufficiently near the bridge is not feasible. The industry requires a more convenient means to measure bridge displacement.
2) The rail industry has not yet established standards for acceptable displacement limits under revenue service traffic. The correlation of displacement to rail safety is not determined. Current limits regarding displacements are oriented toward design analysis. Consequently, the railroads need new limits that reflect the performance of railroad bridges during their service life.

[1] Moreu, F., & LaFave, J. M. (2012). Current Research Topics: Railroad Bridges and Structural Engineering. Newmark Structural Engineering Laboratory Report Series, No. 032 (Also see: http:///hdl.handle.net/2142/34749).

[2] Moreu, F., Jo, H., Li, J., Kim, R., Cho, S., Kimmle, A., Scola, S., Le, H., Spencer, B. F., Jr., & LaFave, J. M. (2015). Dynamic Assessment of Timber Railroad Bridges using Displacements. Journal of Bridge Engineering, 20(10): 04014114.

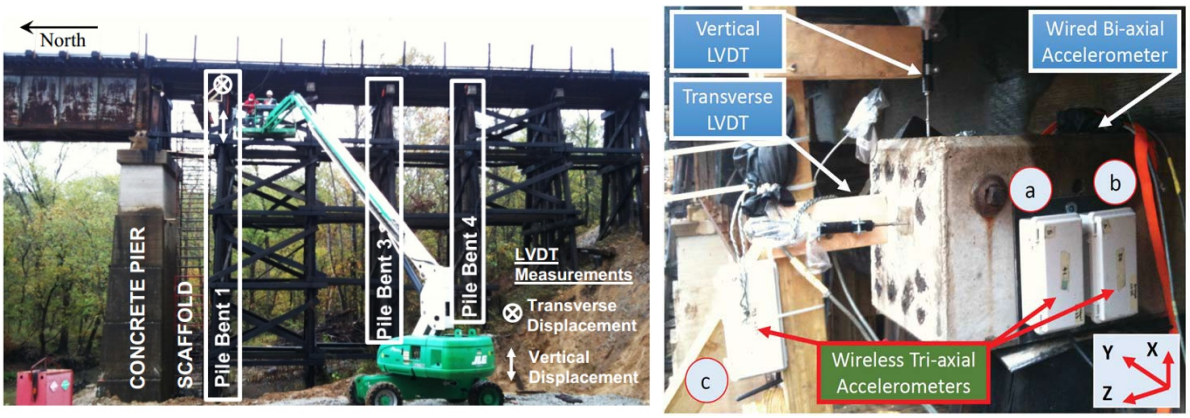

Figure 1.1 Field setup to measure displacements and accelerations

A wireless smart sensor (WSS) is a portable bridge inspection tool that railroad personnel can quickly and easily install, use, and remove. Several full-scale deployments have demonstrated the potential of wireless sensing technology for monitoring highway bridges. For example, the second Jindo Bridge[3] (Figure 1.2a) deployment in Korea, consisting of 113 wireless sensors with 669 sensing channels, is the world largest full-scale wireless smart sensor network for monitoring civil infrastructure. The Government Bridge,[4] a swing-bridge in Illinois, is another example of full-scale and long-term monitoring deployment (Figure 1.2b). In 2013, the research team measured bridge responses of a 310-foot-long steel truss bridge using wireless sensors to obtain global bridge responses under given train loads and speeds.[5] This effort demonstrated the feasibility of campaign bridge monitoring under revenue service traffic (Figure 1.3). These hardware and software innovations create a flexible smart sensor framework for full-scale, autonomous structural health monitoring (SHM) system.

Figure 1.2 Bridges monitored by researchers: (a) Jindo Bridge, (b) Government Bridge

[3] Spencer, B. F., Jr., Cho, S., & Sim, S. H. (2011). Wireless Monitoring of Civil Infrastructure Comes of Age. Structures Magazine, pp. 12-15. (Also see: http://www.structuremag.org/Archives/2011-10/C-Technology-Spencer-Oct11.pdf)
[4] Giles, R. K., Kim, R., Sweeney, S.C., Spencer, B. F., Jr., Bergman, L. A., Shield, C. K., & Olsen, S. (2012). Multimetric Monitoring of a Historic Swing Bridge. Proceedings of the ASCE Structures Congress. (Also see: http://dl.dropbox.com/u/9924653/249_Giles_MultimetricMonitoringHistoricSwingBridge_Final.pdf)
[5] Spencer, B. F., Jr., Moreu, F., & Kim, R. (2015). Campaign Monitoring of Railroad Bridges in High-Speed Shared Corridors using Wireless Smart Sensors. Newmark Structural Engineering Laboratory Report Series, No. 040 (Also see: http://hdl.handle.net/2142/78095)

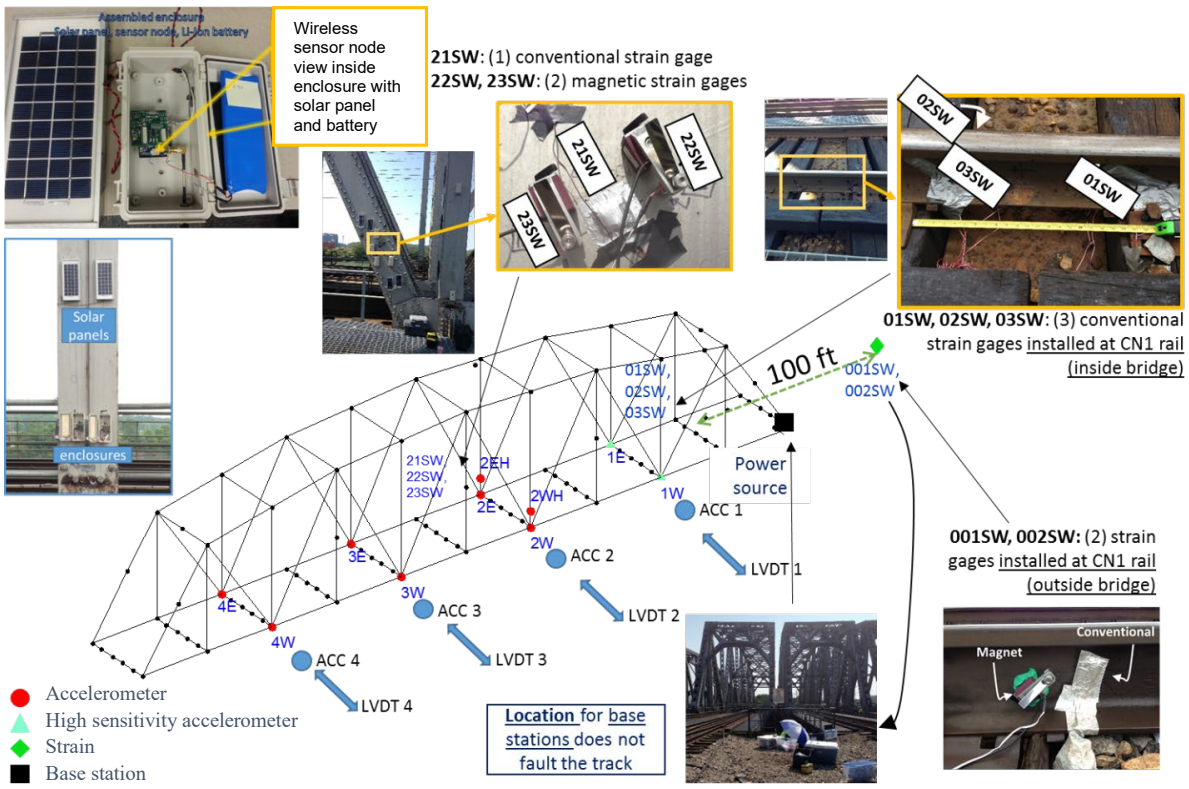

Figure 1.3 Little Calumet River Bridge monitoring (FRA, 2013)

This research extends the studies of Park et al.[6] and Moreu et al.,[7] demonstrating the potential of the direct estimation of dynamic railroad bridge displacements under revenue service traffic. This reference-free displacement estimation method minimizes the difference between the double derivative of the displacement and the acceleration over a finite time interval. This research develops algorithms that can be embedded in a WSS, such as the Imote2 or the Xnode. These results are of interest to railroad researchers, engineers, and administrators for the potential use of technologies offering an objective means to assess bridge conditions.

1.2 Objectives

The primary objective of this research project is to develop a straightforward and cost-effective means to estimate dynamic bridge displacements under revenue service traffic without the need for a fixed reference point. In the U.S., 77 percent of railroad bridges are made of either timber

[6] Park, J., Sim, S., Jung, H., Lee, J., & Spencer, B.F., Jr. (2011). Displacement estimation from acceleration response using smart sensors.; Proceedings of the 2011 World Congress on Advances in Structural Engineering and Mechanics (ASME'11*). Seoul, Korea, 18-22 September.

[7] Moreu, F., Jo, H., Li, J., Cho, S., Kim, R., Spencer, B. F. Jr., & LaFave, J. (2012). Reference-free displacement estimation for structural health monitoring of railroad bridges. AREMA 2012 Annual Conference & Exposition, Chicago.

or steel.[8] Therefore, the proposed system was field-validated for timber trestles and pin-connected steel truss bridges.

In addition, the design of the new reference-free algorithms allows their integration into the wireless system. Railroad personnel can use the WSS system to collect critical data of bridges of the same type but in different conditions and subsequently develop recommendations about service limit states for different bridge types. Figure 1.4 illustrates the system concept. This system will provide railroads with new objective information about the in-service performance of their bridges by estimating the dynamic displacements of existing bridges. Ultimately, this research will improve railroad safety, increase structural reliability, enhance inspection quality, reduce maintenance costs, and help prioritize bridge repairs and replacements.

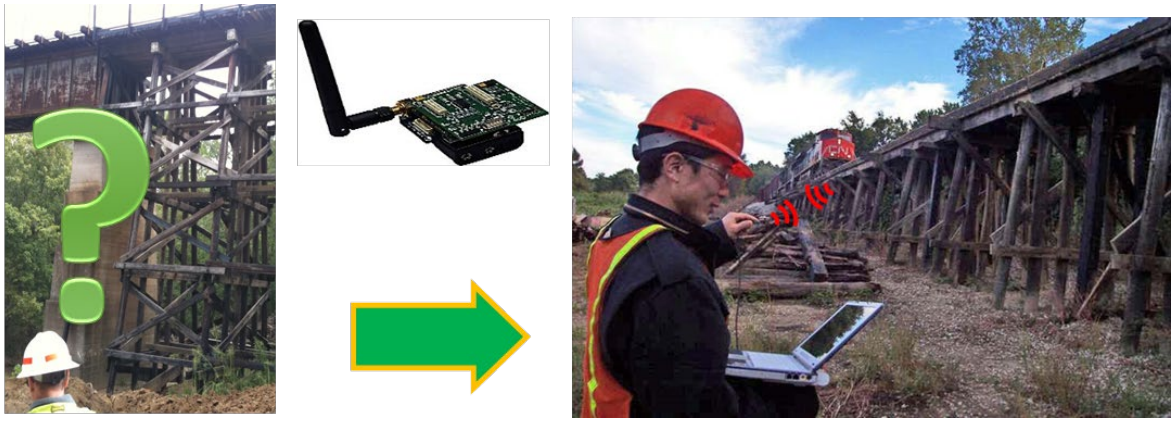

Figure 1.4 Concept of real-time reference-free displacement estimation of railroad bridges under revenue service traffic using WSS

The project has three main objectives:

1) Develop and validate numerically and in the laboratory the reference-free displacement method for collecting real-time displacements of bridges under train loads.
2) Validate displacements estimations on both a timber trestle and a pin connected truss bridge, comparing results with the linear variable differential transformer (LVDT) displacement measurements.
3) Provide quality control and quality assurance throughout the project.

The outputs of this research project were to provide railroads with new objective information about the in-service performance of their bridges that addresses the following needs:

- Safety – Regular campaign monitoring of bridges increases the safety of railroad operations.
- Bridge Management – Bridge replacement prioritization requires quantifiable data about the bridge population to enable rationale decision-making and budget allocation.
- Planning and Transportation – The railroad can better identify the current structural capacity of the bridges within the network.

[8] Federal Railroad Administration. (2008). U.S. Railroad Bridge Superstructure Materials by Length.

- Institutional – Regulatory recommendations, incentives, and penalties associated with bridge management (and liability consequences) to improve the safety of railroad operations.[9]

1.3 Overall Approach

This project included the development and validation of reference-free algorithms in the laboratory in addition to the field validation of the system on in-service bridges. The results and developments were coordinated with the Federal Railroad Administration (FRA) throughout the 15-month period of the project. This work builds on prior outcomes of FRA-funded research with the objectives of improving safety of railroad bridges and overall rail operations.

1.4 Scope

To achieve the goals and objectives of this project, researchers complete seven critical tasks over the project's 15-month duration (see Figure 1.5):

1) Interviews with industry experts and a review of available data and information and past research efforts
2) Develop reference-free displacement estimation algorithms using measured accelerations, including parametric analyses of the filter.
3) Numerical validation using Bluford Bridge field data and a laboratory validation of the algorithm using hydraulic motion simulator to recreate measured bridge motions
4) Selection of bridges to be monitored in coordination with industry partners and preliminary assessment of the bridges
5) Instrumentation and monitoring of timber trestle and pin-connected steel truss bridges under revenue service traffic
6) Comprehensive technical report and presentation to industry. Research publications will be available in the Newmark Structural Engineering Laboratory Report Series, contained in the University of Illinois digital repository, IDEALS.
7) Quality assurance of the overall project through quarterly meetings and reports, and continuous coordination with the project manager

[9] FRA. (2010, July 15). Bridge Safety Standards.

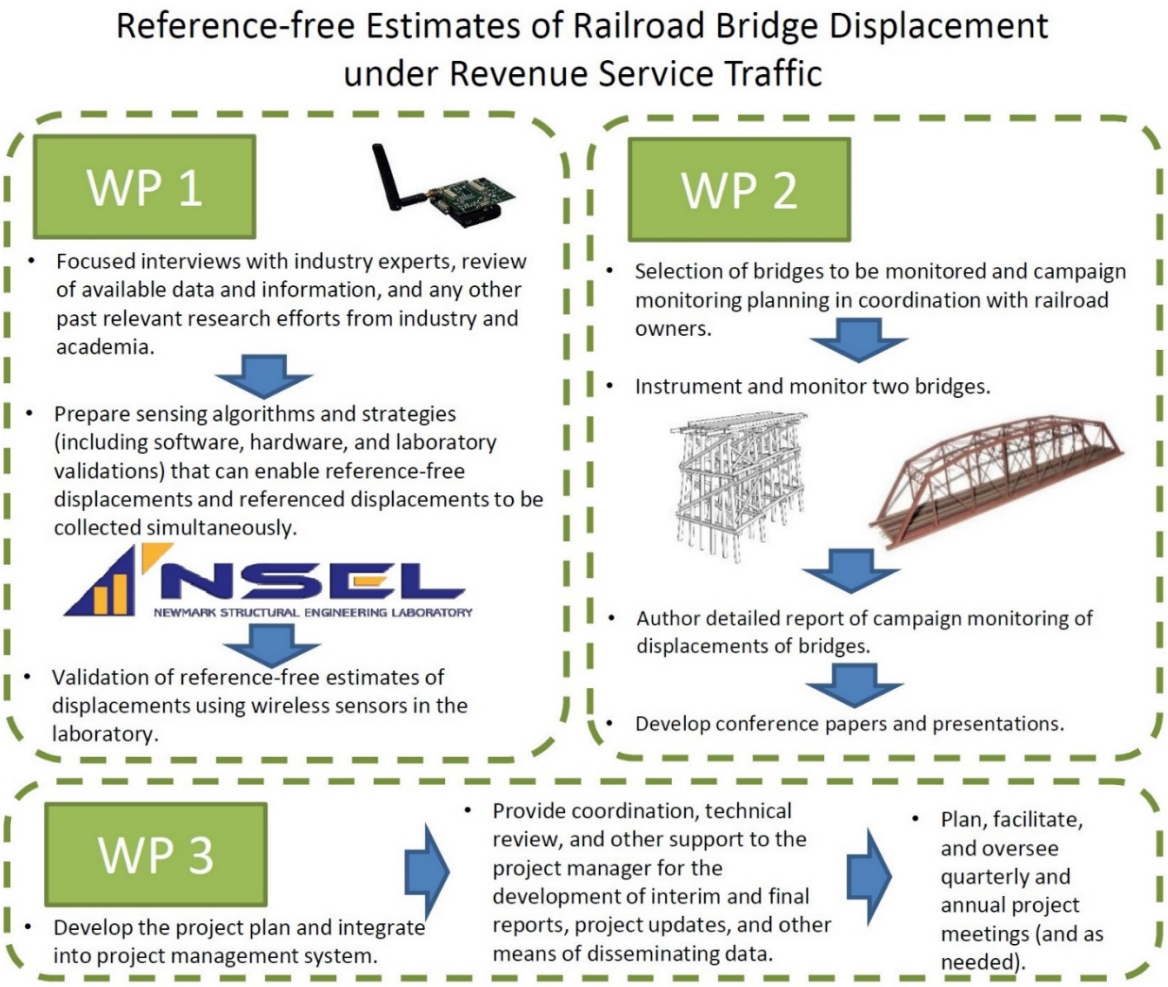

Figure 1.5 Technical approach of the project

1.5 Organization of Report

This report presents the motivation for the research, the results of a survey of the railroad industry, the developed algorithm to estimate reference-free displacement from measured accelerations, a comparison with the previous approach, numerical and laboratory validations, field implementation and deployment, and conclusions and recommendations for future studies.

Section 2 discusses industry desires for bridge displacement data. Section 3 presents the available methods for displacement estimation, shows the shortcomings of previous approaches, and presents a new method for reference-free displacement estimation using measured accelerations. Section 4 details the bridges tested in this project. Section 5 describes the use of a vision-based displacement measurement method that was used as a reference for the new accelerometer-based method. Section 6 describes the tests of the reference-free displacement measurement technique. Section 7 contains the report conclusions and a technology gap analysis, and Section 8 provides recommendations for additional research.

2. Motivation for Bridge Displacement Estimation

This section discusses some of the current concerns of railroad industry experts regarding bridge displacements under revenue service train loads.

2.1 Summary of Survey of Experts

In 2014, the research team surveyed 20 railroad industry experts to assess their concerns regarding the state of repair of railroad bridges; Figure 2.1 shows their affiliations. Table 2.1 contains the survey questionnaire.

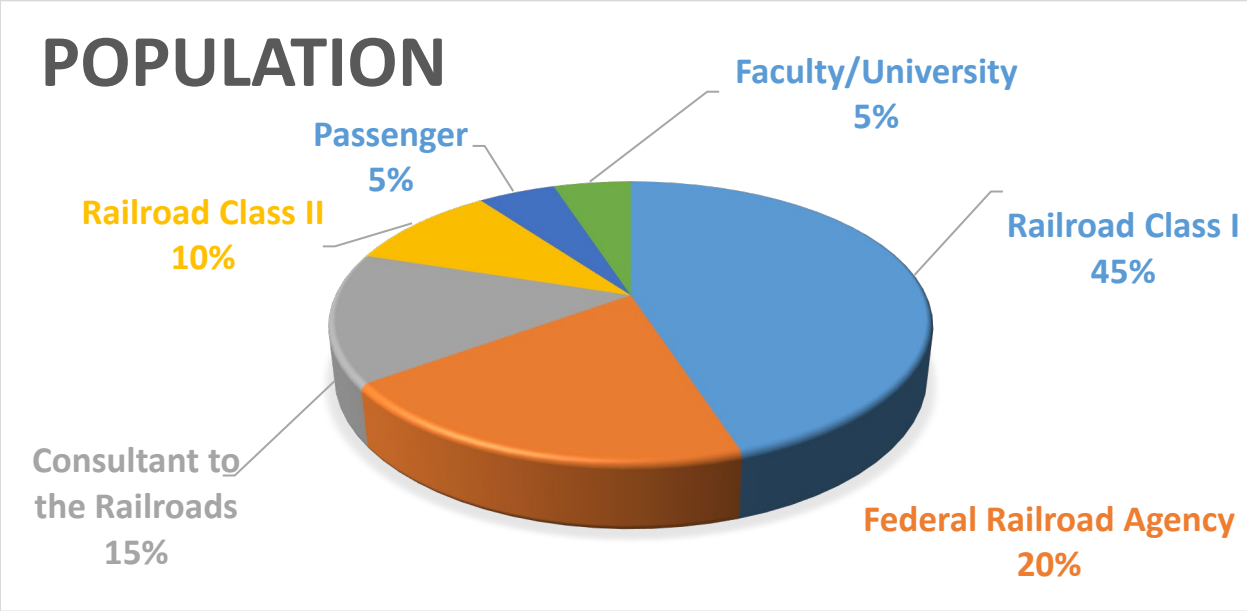

Figure 2.1 Overview of the population of bridge experts surveyed

Table 2.1 Survey Questionnaire

1. WHICH TYPE OF RAILROAD BRIDGES ARE YOU MOST WORRIED ABOUT? (WHICH TYPES OF BRIDGES CONSUME THE LARGEST PORTION OF YOUR BRIDGE BUDGET?)
2. WHY ARE YOU MOST WORRIED ABOUT THIS/THESE TYPE/S OF BRIDGE/S?
3. WHAT/WHERE IS THE MAIN PROBLEM WITH THIS/THESE TYPE/S OF BRIDGE/S?
4. WHY IS IT A PROBLEM? WHAT CAN HAPPEN IF YOU MISS IT?
5. WHAT WOULD YOU MEASURE TO CONTROL/ MONITOR/ UNDERSTAND THIS PROBLEM?
6. WHERE WOULD YOU MEASURE IT?
7. HOW OFTEN WOULD YOU MEASURE IT?
8. WHICH LIMIT/S WOULD YOU PROPOSE FOR THIS MEASUREMENT? (VARIOUS LIMITS FOR VARIOUS LEVELS OF PERFORMANCE ARE POSSIBLE)

9. ANY EXAMPLE OF ANY MEASUREMENT UNDER TRAFFIC IN THE PAST THAT INDICATED A CONCERN FOR ANY BRIDGE TYPE?
10. ANY COMMENT/SUGGESTION/QUESTION TO ADD

Figure 2.2 shows the types of bridges of highest concern to the industry based on this survey. In addition, the survey responses indicated that the following issues are of particular interest:

- Timber pile displacements in all directions
- Timber beam displacements in vertical direction
- Steel beam displacements in all directions
- Steel crack width on floor beams
- Pin connected trusses eye-bar vibration
- Permanent settlement in large piers
- Scouring for all types of bridges

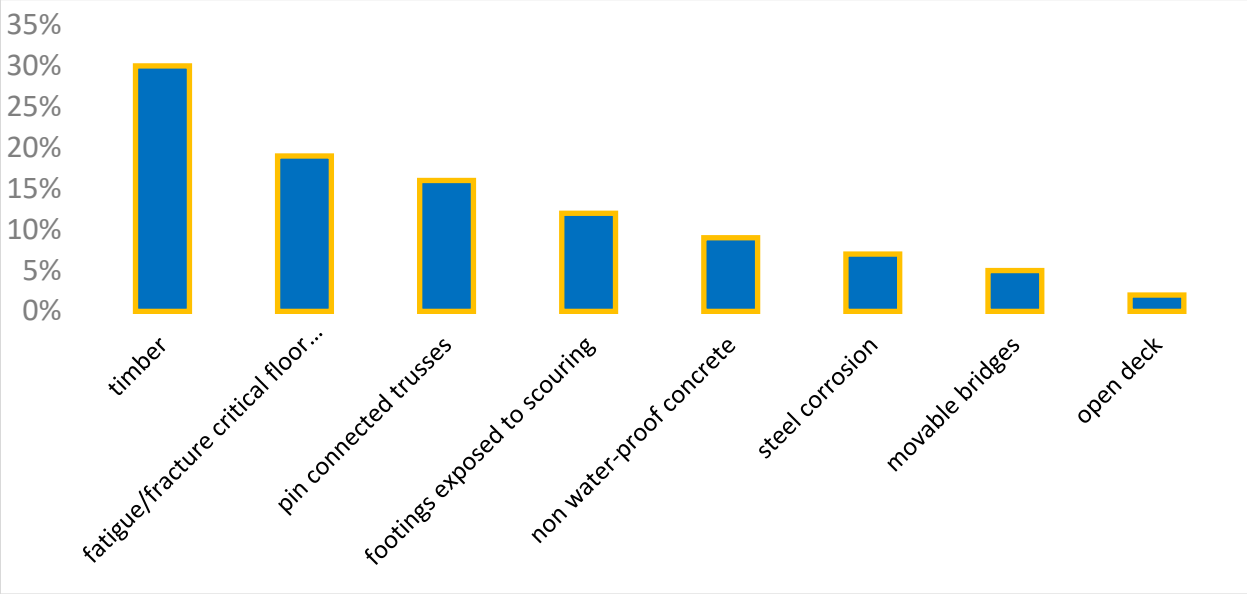

Figure 2.2 Railroad bridge types that are a top concern to the railroad industry

2.2 General Concerns with Bridges

The industry recognizes that timber bridges decay faster than steel and are in the poorest overall condition. Figure 2.3 shows a typical timber trestle bridge. Timber bridges offer significant redundancy, but when changing the load path, the load distributes to fewer sections, resulting in accelerated bridge decay.

Figure 2.3 Typical timber trestle bridge

For smaller railroads (Class II and Class III), timber bridges account for 52 percent of bridge mileage. Most of these bridges were designed and built for 263,000-lb. cars, but are now carrying 286,000-lb. cars. The cost of replacement of a timber trestle bridge exceeds $6,500 per foot. Class II railroads spend from $1 to $3 million per year for timber replacements. Meanwhile, Class I railroad maintenance, repair, and replacement budgets can exceed $60 million per year. Infrastructure and bridge investments represent a significant element of a railroad's annual maintenance budget.

Another industry concern is steel pin-connected truss bridges. Figure 2.4 shows a typical steel pin-connected truss bridge. Lateral and vertical displacements that exceed a certain fraction of the design values, for example $L/640$ where L equals the span length, can be a serviceability limit. A possible criterion is that if the displacement achieves 25 percent of the design limit, the bridge needs a comprehensive inspection; if it achieves 50 percent of the limit, it requires repairs; and if it achieves 75 percent of the limit, it requires traffic reduction. In addition, for pin-connected trusses, changes in the natural frequencies of eye bars can indicate decay in the connection and assist in prioritizing replacements.

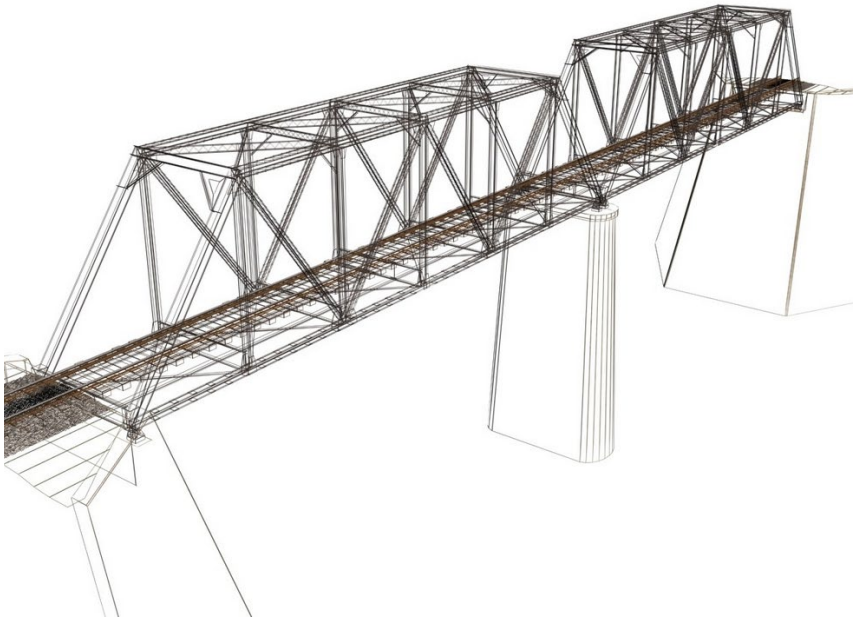

Figure 2.4 Typical steel pin-connected truss bridge

2.3 Review of Existing Displacement Limits

Table 2.2 and Table 2.3 show current displacement limits for timber bridges and steel bridges, respectively.[10] These limits are for design purposes only. Railroad engineers recognize and agree that these limits are not appropriate for the evaluation of existing bridges. Moreover, AREMA has yet to establish limits for transverse displacement of timber bridges.

Table 2.2 Design displacement limits in AREMA for timber bridges

Timber	Limit	AREMA section	AREMA page	Year
Vertical	*L*/250	3.1.15	7-3-5	2009

[10] AREMA (2014); Manual for Railway Engineering; April.

Table 2.3 Design displacement limits in AREMA for steel bridges

Steel	Limit	AREMA section	AREMA page	Year
Vertical	*L*/640	1.2.5.b	7-3-5	2001/2010
Transverse (tangent track)	3/8” per 62 ft.	1.2.5.c	15-1-12	2001/2010
Transverse (curved track)	¼” per 31 ft.	1.2.5.c	15-1-12	2001/2010

The vertical design limit is 5/8-inch for a 13-foot span; displacements higher than 3/4-inch could be a concern. On the other hand, no limits exist for transverse displacements; Moreu et al.[2] suggested that transverse displacements greater than *H*/250, where *H* equals the pile height (above ground) can be an indication of needs for further inspection; tall and long timber trestles are of concern. Further monitoring of these bridges is needed to set a baseline.

Railroads want to explore limiting the displacement of railroad bridges under freight trains. For example, excessive transverse displacement can indicate overstressed portions of the timber trestle resulting from poor pile condition or poor cross-bracing.

Little information is available regarding lateral displacements of timber bridges. Consensus among interviewed engineers was lacking as to whether it is safer to have a train sitting on the bridge or crossing the bridge at a very fast speed. In general, timber bridges that move excessively should be inspected or re-rated.

No set metrics or limits are available regarding the displacements of bridges under in-service trains, except for design. Railroads and researchers have a general interest in collecting more displacements in the field, which can inform what those limits should be to prioritize bridge replacements.

3. Reference-free Displacement Estimation

This section presents the available methods for displacement estimation, shows the shortcomings of previous approaches, and presents a new method for reference-free displacement estimation using measured accelerations particularly suitable for implementation on WSS.

3.1 Literature Review on Displacement Estimation

Displacement measurements are useful information for railroad bridge monitoring because they directly reflect the structural condition. Displacement responses from a structure can be obtained by (1) direct contact-type, (2) non-contact type, and (3) reference-free methods (see Figure 3.1). A LVDT is a type of sensor employed in contact type measurements. The accuracy of this type of method is guaranteed, but installation is difficult and requires a connection between the structure and a fixed reference. Non-contact methods can measure displacement of a structure from a remote location. Examples include laser Doppler vibrometers (LDV), and vision-based systems.[11,12,13] However, measurement accuracy is dependent on the device mounting condition on a reference point. Reference-free methods that do not rely on a fixed reference point are attractive alternatives to existing measurement techniques. A Global Positioning System (GPS) is one example of a reference-free method, but the accuracy of the device (±1.5 mm) is not appropriate to most short-span bridges.[14]

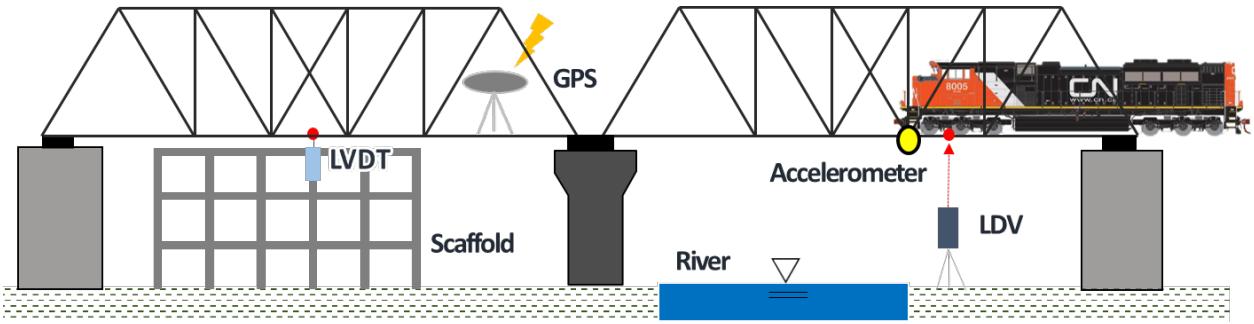

Figure 3.1 Illustration of displacement measurement for a bridge structure

[11] Nassif, H.H., Gindy, M., & Davis, J. (2005). Comparison of laser Doppler vibrometer with contact sensors for monitoring bridge deflection and vibration. Ndt & E International, 38(3): 213-218.
[12] Park, J.W., Lee, J. J., Jung, H. J., & Myung, H. (2010). Vision-based displacement measurement method for high-rise building structures using partitioning approach. Ndt & E International, 43(7): 642-647.
[13] Lee, J.J. & Shinozuka, M. (2006). A vision-based system for remote sensing of bridge displacement. Ndt & E International, 39(5): 425-431.
[14] Celebi, M. & Sanli, A. (2002). GPS in Pioneering Dynamic Monitoring of Long-Period Structures. Earthquake Spectra, 18(1): 47-61.

Other reference-free displacement estimation methods use acceleration[15, 16, 17] and strain.[18] Researchers commonly use accelerometers in dynamic testing of structures because of the ease of installation and the relatively low cost, thus this method has the potential to be widely adopted. Displacement estimation using acceleration measurements is theoretically feasible because the double integration of acceleration is equal to displacement. The accuracy of these calculations is affected by the noise present in the measured acceleration. Figure 3.2 shows displacement estimation using the integration approach. As shown, the estimation diverges from the actual displacement because this method amplifies the low-frequency noise in the acceleration.

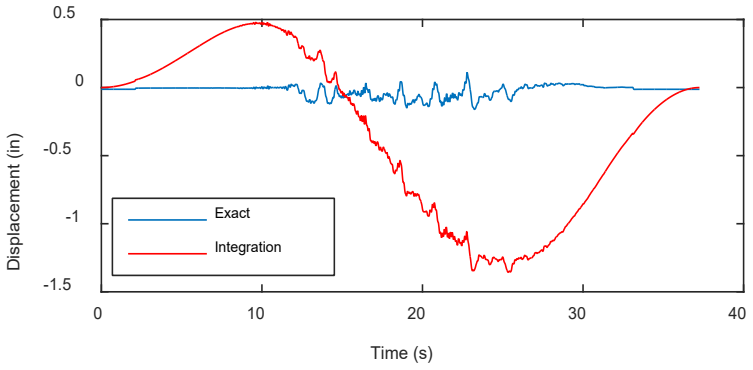

Figure 3.2 Displacement estimation using integration

As an alternative to the integration method, previous researchers[17, 18, 19, 19] have defined a minimization problem with Tihkonov regularization with the following objective function:

$$\Pi(u) = \frac{1}{2}\int_{T_1}^{T_2}\left(\frac{d^2u}{dt^2} - \bar{a}\right)^2 dt + \frac{1}{2}\beta^2\int_{T_1}^{T_2} u^2 dt \tag{1}$$

where u is the estimated displacement, $\bar{a}$ is the measured acceleration, and β is the Tihkonov regularization factor. The problem is discretized on the time interval $T_1 < t < T_2$ using a time step Δt to obtain the following discrete version of the minimization problem:

$$\min_{\mathbf{u}} \Pi(\mathbf{u}) = \frac{1}{2}\left\|\mathbf{L}\mathbf{u} - (\Delta t)^2 \mathbf{L}_a \bar{\mathbf{a}}\right\|_2^2 + \frac{\beta^2}{2}\|\mathbf{u}\|_2^2 \tag{2}$$

---

[15] Hong, Y. H, Kim, H.K., & Lee, H.S. (2010). Reconstruction of dynamic displacement and velocity from measured accelerations using the variational statement of an inverse problem. Journal of Sound and Vibration, 329(23): 4980-5003.
[16] Lee, H.S., Hong, Y.H., & Park, H.W. (2010). Design of an FIR filter for the displacement reconstruction using measured acceleration in low-frequency dominant structures. International Journal for Numerical Methods in Engineering, 82(4): 403-434.
[17] Park, K.T., Kim, S.H., Park, H.S., & Lee, K.W. (2005). The determination of bridge displacement using measured acceleration. Engineering Structures, 27(3): 371-378.
[18] Kang, L.H., Kim, D.K., & Han, J.H. (2007). Estimation of dynamic structural displacements using fiber Bragg grating strain sensors. Journal of Sound and Vibration, 305(3): p. 534-542.
[19] Park, J.W, Sim, S.H., & Jung, H.J. (2013). Development of a wireless displacement measurement system using acceleration responses, Sensors, 13(7): 8377-8392.

where $\mathbf{u}$ and $\bar{\mathbf{a}}$ are vectors of length $2k+1$ that contains the displacements and accelerations, respectively. $\|.\|_2$ is the 2-norm of the corresponding vector. $\mathbf{L}_a$, $\mathbf{L}_c$ and $\mathbf{L}$ are the following matrices whose dimensions are $(2k+1)\times(2k+1)$, $(2k+1)\times(2k+3)$ and $(2k+1)\times(2k+3)$, respectively:

$$\mathbf{L}_a = diag\left(\frac{1}{\sqrt{2}}, \underbrace{1,...,1}_{2k-1}, \frac{1}{\sqrt{2}}\right) \tag{3}$$

$$\mathbf{L}_c = \begin{bmatrix} 1 & -2 & 1 & & & \\ & 1 & -2 & 1 & \mathbf{0} & \\ & & & \ddots & & \\ & \mathbf{0} & & & 1 & -2 & 1 \end{bmatrix} \tag{4}$$

$$\mathbf{L} = \mathbf{L}_a \mathbf{L}_c \tag{5}$$

Using these results, the exact solution of the discrete minimization problem is given by:

$$\mathbf{u} = (\Delta t)^2 \left(\mathbf{L}^T\mathbf{L} + \beta^2\mathbf{I}\right)^{-1} \mathbf{L}^T\mathbf{L}_a\bar{\mathbf{a}} = (\Delta t)^2 \mathbf{C}\,\bar{\mathbf{a}} \tag{6}$$

where $\mathbf{I}$ is the identity matrix with consistent dimensions, and β is an empirically obtained regularization factor. Because the boundary conditions affect the solution but are unavailable, researchers have employed a moving window technique, which consists of selecting only the middle point of the time window as the solution, because it is the point less affected by the boundary conditions of the window. Defining the vector $\mathbf{c}_{k+1+p} = \mathbf{C}_{k+2,k+1+p}$, that is the middle row of the matrix **C**, the solution for the displacement then reduces to:

$$u(t) = u_{k+1} = (\Delta t)^2 \sum_{p=-k}^{k} \mathbf{c}_{k+1+p}\,\bar{\mathbf{a}}(t + p\Delta t) \tag{7}$$

One concern is that the solution of the problem depends on the size of the time window and the regularization factor. To address this problem, researchers have optimized the length of the time window and the regularization factor empirically.

3.2 Filter Development for the Reference-free Displacement Estimation

3.2.1 Comparison of Accuracy Function in Frequency Domain

The previous approach for displacement estimation is straightforward but has significant weaknesses. The frequency response function (FRF) is the ratio between the Fourier transform of the output and the input, which in this case are the displacement and acceleration, respectively. The FRF of the double integrator is $-\omega^2$; thus, an accuracy function can be defined as the magnitude of the ratio between the transfer function $H_{u\bar{a}}(\omega)$ and the Fourier transform of the perfect integrator, as shown in Eq. (8):

$$H^{accu}(\omega) = \left| H_{u\bar{a}}(\omega) / \omega^2 \right| \tag{8}$$

Figure 3.3 shows the accuracy function for the previous method (i.e., Eq. (8)). To eliminate the negative effect of low-frequency noise, the accuracy function should be zero in this region, which it is. However, the ripples in the frequency domain and divergence at high frequencies can cause significant errors when applying this method.

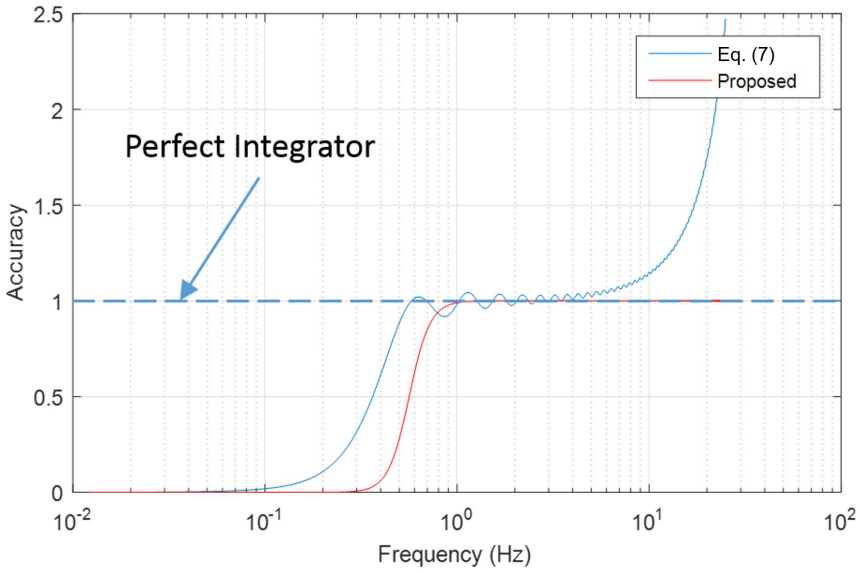

Figure 3.3 Comparison of accuracy function

3.2.2 Problem Formulation

Another approach is to obtain the minimum for the Tihkonov regularization problem in Eq. (1), consequently the first variation of the functional should be zero:[17]

$$0 = \delta\Pi(u) = \int_{T_1}^{T_2} \left(\frac{d^2u}{dt^2} - \bar{a} \right) \frac{d^2\delta u}{dt^2} dt + \beta^2 \int_{T_1}^{T_2} u\,\delta u\, dt \tag{9}$$

Applying integration by parts twice and simplifying the expression yields:

$$0 = \delta\Pi(u) = \int_{T_1}^{T_2} \left(\frac{d^4u}{dt^4} - \frac{d^2\bar{a}}{dt^2} + \beta^2 u \right) \delta u\, dt + \left(\frac{d^2u}{dt^2} - \bar{a} \right) \frac{d\delta u}{dt} \Bigg|_{T_1}^{T_2} - \left(\frac{d^3u}{dt^3} - \frac{d\bar{a}}{dt} \right) \delta u \Bigg|_{T_1}^{T_2} \tag{10}$$

The corresponding governing equation, without the boundary conditions, is:

$$\frac{d^4u}{dt^4} + \beta^2 u = \frac{d^2\bar{a}}{dt^2},\ T_1 < t < T_2 \tag{11}$$

The associated boundary conditions are prescribed displacements and velocities. These have a significant impact on the solution of the governing equation, but the boundary conditions are not readily obtained.

3.2.3 Frequency-Domain Analysis and General Filter

Applying the Fourier Transform to the governing equation yields:

$$(i\omega)^4 F(u) + \beta^2 F(u) = (i\omega)^2 F(\bar{a}) \tag{12}$$

Hence, the FRF for Eq. (12) is:

$$H_{u\bar{a}}(\omega) = \frac{F(u)}{F(\bar{a})} = \frac{(i\omega)^2}{(i\omega)^4 + \beta^2} = -\frac{\omega^2}{\omega^4 + \beta^2} \tag{13}$$

The accuracy function is given by:

$$H^{accu}(\omega) = H_{u\bar{u}}(\omega) = (i\omega)^2 H_{u\bar{a}}(\omega) = \frac{\omega^4}{\omega^4 + \beta^2} \tag{14}$$

The problem can be generalized to the order *n* instead of 2, as Eq. (15) shows, by adopting the generalized Butterworth filter.[20] Then, the accuracy function and FRF can be expressed as:

$$H^{accu}(\omega) = H_{u\bar{u}}(\omega) = (i\omega)^2 H_{u\bar{a}}(\omega) = \frac{\omega^{2n}}{\omega^{2n} + \beta^n} \tag{15}$$

$$H_{u\bar{a}}(\omega) = \frac{H^{accu}(\omega)}{(i\omega)^2} = \frac{(i\omega)^{2n-2}}{(i\omega)^{2n} + \beta^n} = -\frac{\omega^{2n-2}}{\omega^{2n} + \beta^n} \tag{16}$$

where *n* is the order of the filter, which could be any integer greater than 1; and β is the regularization factor, which is a positive real number. Both parameters define completely the behavior of this filter.

Regularization factor

The accuracy function depends on the regularization factor β. The dependence on this factor is replaced by defining the target accuracy α_T, such that the accuracy function evaluated at the target frequency f_T is defined as the target accuracy α_T, i.e.:

$$H^{accu}(\omega_T) = H^{accu}(2\pi f_T) = \alpha_T \tag{17}$$

---

[20] Oppenheim A. V., & Schafer, R. W. (1989). Discrete-Time Signal Processing. Prentice Hall, Englewood Cliffs, NJ.

The regularization factor β depends on the target frequency f_T and the target accuracy α_T by means of the following expression:

$$\alpha_T = \frac{(2\pi f_T)^{2n}}{(2\pi f_T)^{2n} + \beta^n} \Rightarrow \beta = \sqrt[n]{\frac{1-\alpha_T}{\alpha_T}}(2\pi f_T)^2 \tag{18}$$

The target accuracy should take values between 0 and 1, not inclusive. If the target accuracy is zero, the regularization factor is infinite; if the target accuracy is one, the filter does not converge, because the regularization factor is equal to zero.

Fixing the order and target frequency of the accuracy function, the effect of the target accuracy α_T can be analyzed. Figure 3.4 shows the effect of the target accuracy on the accuracy function for fixed order.

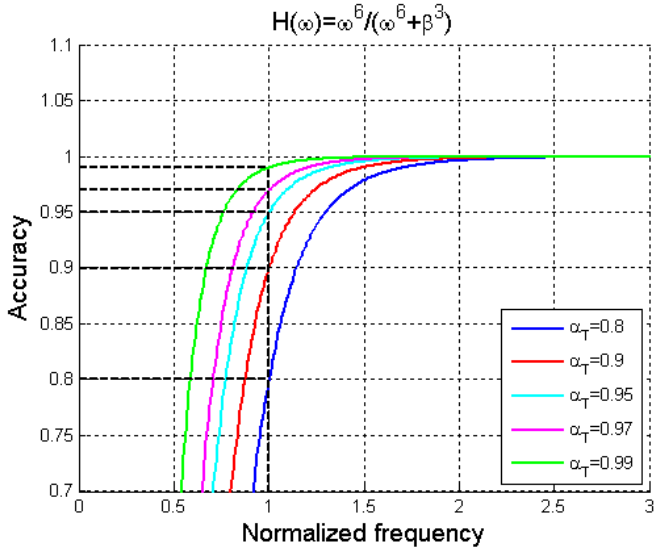

Figure 3.4 Accuracy function for different target accuracy

Values of the target accuracy between 0.80 and 0.99 achieve good results on the filter for second order;[21] empirically, this result also applies for all orders.

Filter order

Figure 3.5 shows the effect of the filter order on the accuracy function. As the filter order increases, the transition area is steeper and the filter is better suited to suppress the noise. However, as the order increases, the corresponding filter becomes longer. Moreover, as the filter order increases, the filter converges more rapidly, as Figure 3.5b demonstrates. In general, a filter order larger than 2 and target accuracy of 0.99 for low target frequencies yield good results.

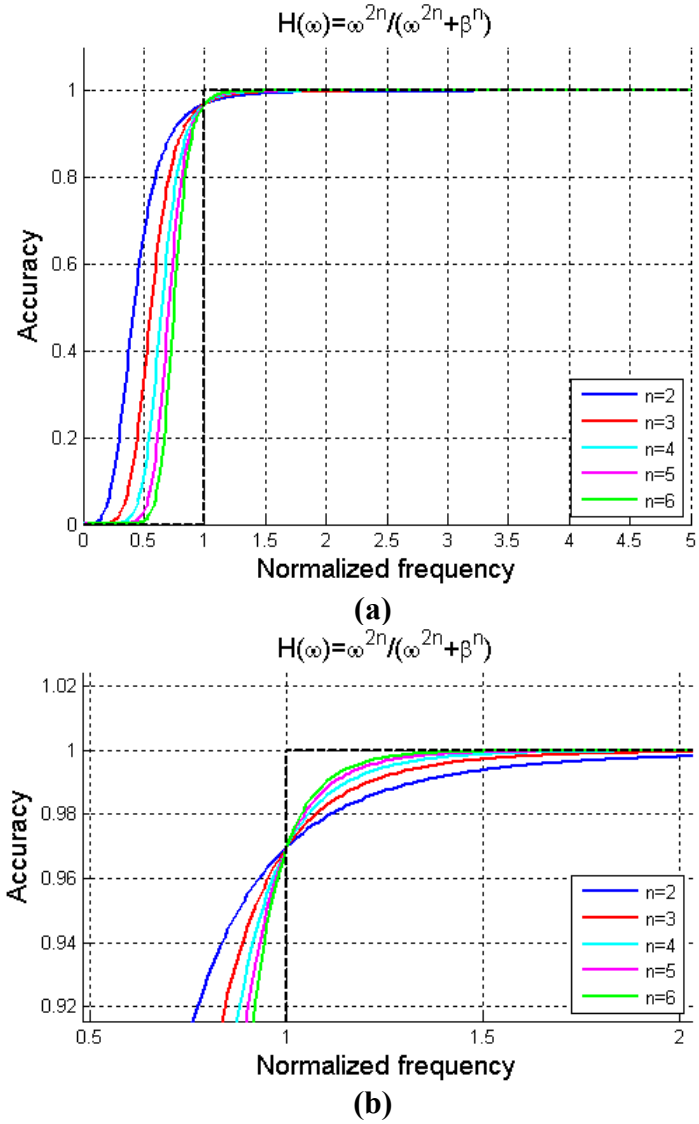

Figure 3.5 Accuracy function for different orders

3.2.4 Continuous-time Analysis

The corresponding transfer function represents the filter in the Laplace domain. In the current case, the transfer function, called "type 1" is:

$$H_1(s) = \frac{s^{2n-2}}{s^{2n} + \gamma} \tag{19}$$

For comparison, consider the following transfer function called "type 2":

$$H_2(s) = \frac{s^{2n-2}}{\left(s^2 + 2\zeta_f \omega_f s + \omega_f^2\right)^n} \tag{20}$$

where ω_f and ζ_f are the frequency and damping ratio of the "type 2" filter, respectively. The type 2 filter has a transition zone where the phase angle is different from zero, which implies delays on the displacement estimation. For the type 2 filter, best results are obtained by defining the damping ratio equal to 0.707, and the filter frequency using the following expression:

$$\omega_f = \omega_T \sqrt[4]{\frac{1-\sqrt[n]{\alpha_T^2}}{\sqrt[n]{\alpha_T^2}}} \tag{21}$$

Figure 3.6 shows the Bode plot for both types of filter for different orders; the type 2 filter has 0.707 of damping ratio, and frequency equal to the target frequency. The proposed filter (type 1) achieve better values for the magnitude, which are close to 1 for frequencies equal or higher than the target frequency. Moreover, the phase is equal to zero. The type 2 filter has both magnitude and phase deviations.

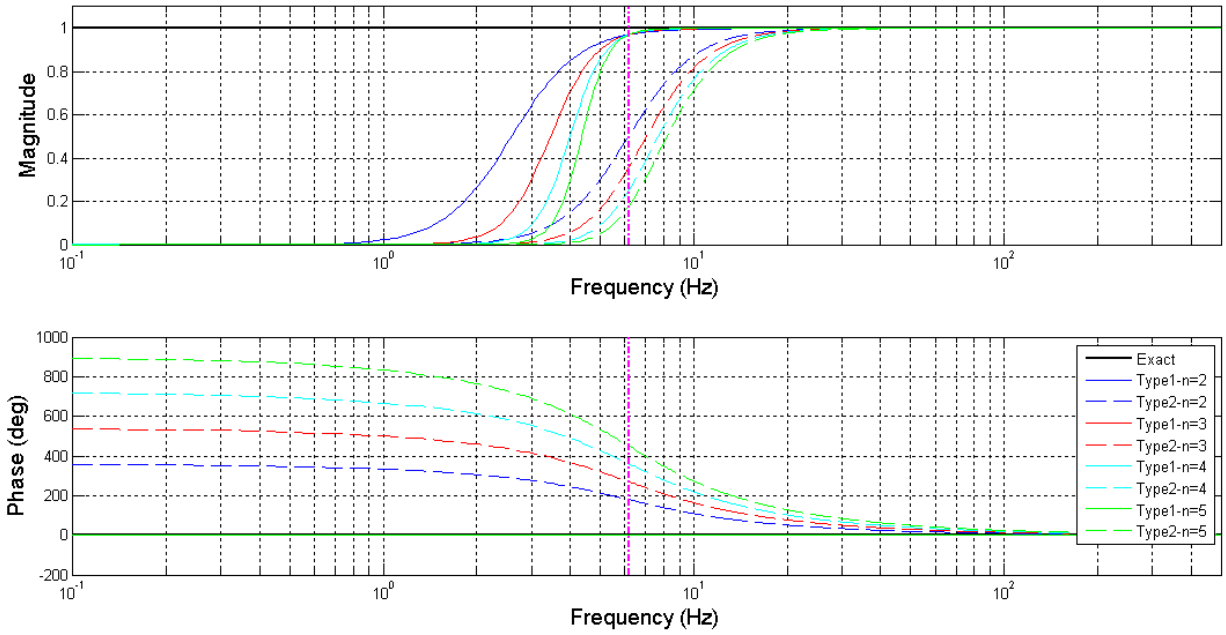

Figure 3.6 Bode plot of the filter for different orders, $\zeta_f = 0.707$, $\omega_f = \omega_T$

Stability of the filter transfer function requires that the poles to have negative real parts. Figure 3.7 shows the poles for both types of filters for different orders; it also shows the different regions of stability and instability. Filter type 2 has repeated poles, all of which are stable.

Although type I filter yields better results than filter type 2, the former is unstable. The next subsection describes an approach to resolve this problem.

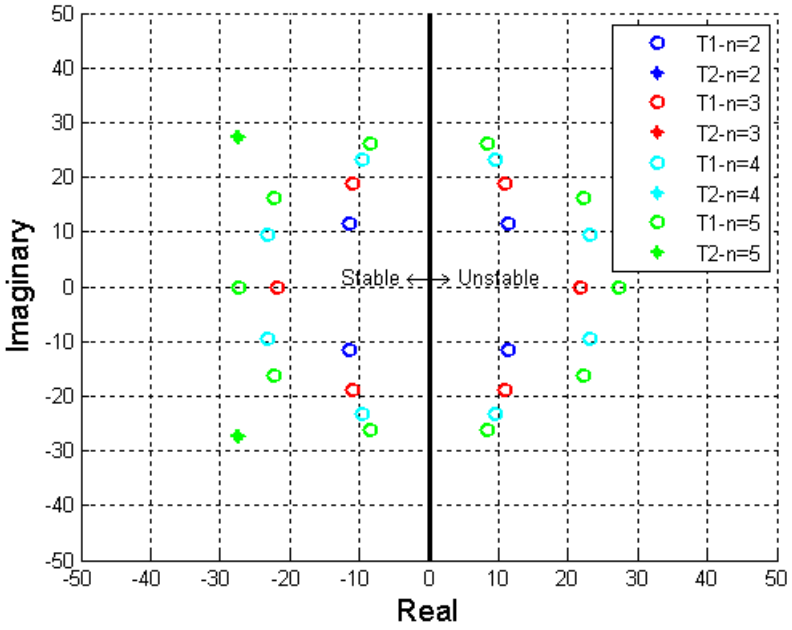

Figure 3.7 Poles of the filter for different orders

3.2.5 Definition of the FIR Filter and Parametric Analysis

Due to instability issues of the filter in the continuous-time representation, a digital FIR filter type I with a generalized linear phase was considered. A vector of coefficients **c** of length $2k + 1$ represents the FIR filter. The relation between the measured acceleration and the estimated displacement is:

$$u(t) = (\Delta t)^2 \sum_{p=-k}^{k} c_{k+1+p}\, \bar{a}(t + p\Delta t) \tag{22}$$

The time window, where the FIR filter acts, is equal to:

$$T = \frac{2k}{f_s} \tag{23}$$

Then, the FRF and the accuracy function are:

$$H(f) = (\Delta t)^2 \sum_{p=-k}^{k} c_{k+1+p} e^{i2\pi pf\Delta t} = (\Delta t)^2 \left(c_{k+1} + 2\sum_{p=1}^{k} c_{k+1+p} \cos(2\pi pf\Delta t) \right) \tag{24}$$

$$H^{accu}(f) = -(2\pi f\Delta t)^2 \left(c_{k+1} + 2\sum_{p=1}^{k} c_{k+1+p} \cos(2\pi pf\Delta t) \right) \tag{25}$$

Hence, the coefficients of the FIR filter satisfy the following expression:

$$c_{p+k+1} = f_s \int_{-fs/2}^{fs/2} H_{u\bar{a}} e^{i2\pi f \Delta t p} df = -\frac{f_s}{2\pi^2} \int_0^{fs/2} \frac{f^{2n-2}}{f^{2n} + \lambda^{2n} f_T^{2n}} \cos(2\pi p f \Delta t) df \tag{26}$$

The FIR filter depends on the target accuracy, the target frequency, and the order as before, but now also depends on the length of the time window. To better assess the influence of the time window length, researchers normalized the time window length by defining it as a fixed number N_w times the target period T_T. Then, the number of points of the filter $2k+1$ is a function of the normalized time window length N_w, the target frequency, and the sampling frequency:

$$T = N_w T_T = \frac{N_w}{f_T} \Rightarrow k = N_w \frac{f_s}{2 f_T} \tag{27}$$

Figure 3.8 shows the effect of the normalized window length on the accuracy function for a fourth-order filter with 0.99 of target accuracy. For arbitrary normalized window length, the accuracy function has a big repulse or divergence after the target frequency.

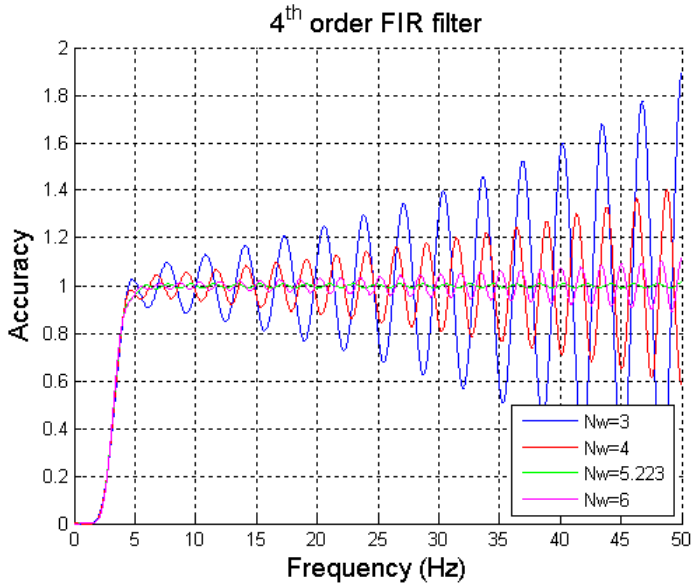

Figure 3.8 Accuracy function for arbitrary normalized window length

The FIR filter coefficients are the truncated Fourier series representation of the FRF, hence the Gibbs' phenomenon occurs. To diminish the Gibbs' phenomenon, the time window should be such that the coefficients in time-domain end at zero. Figure 3.9 shows the coefficients of the infinite (IIR) filter in the time-domain and its respective zeros. All pairs of zeros in the time-domain define different normalized window lengths.

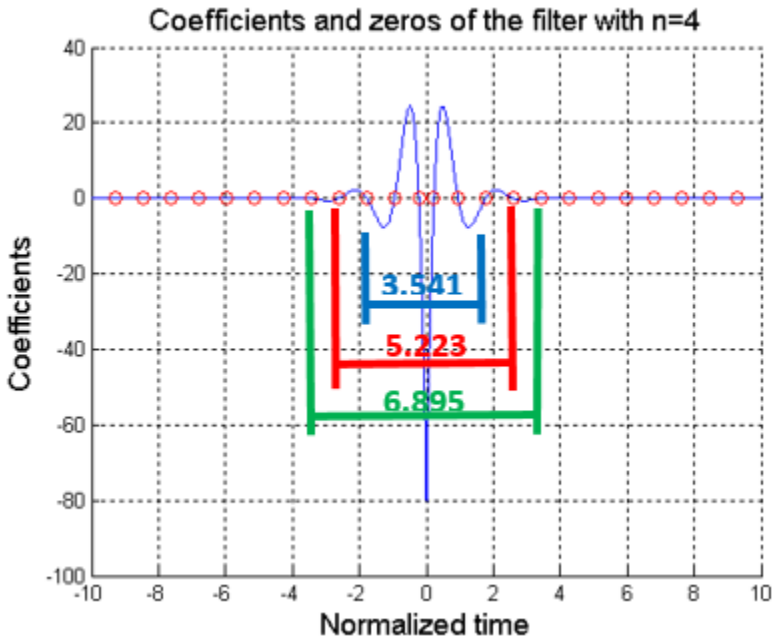

Figure 3.9 Coefficients of the infinite filter in the time domain

Figure 3.10 shows the effect of the optimized normalized window length on the accuracy function for a fourth order filter with 0.99 of target accuracy, which depends on the number of zeros retained.

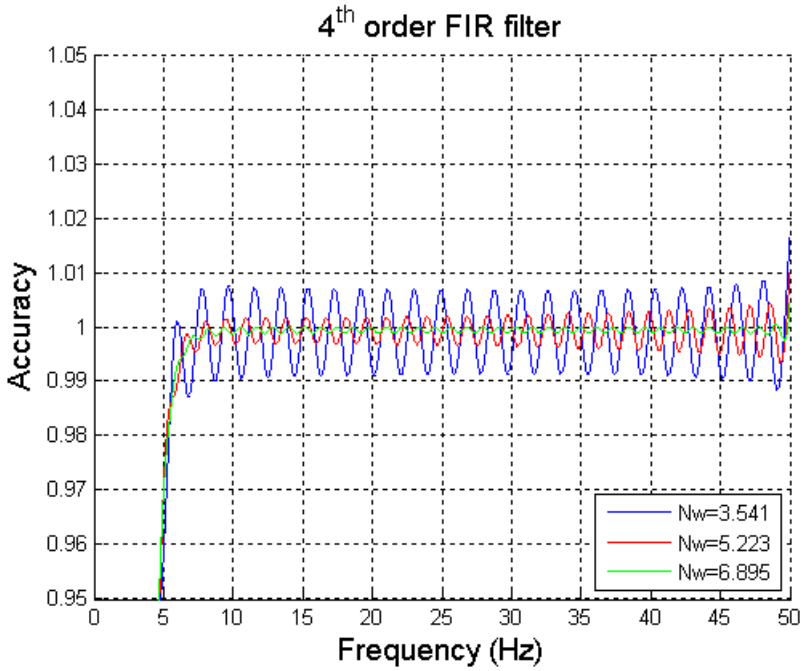

Figure 3.10 Accuracy function for optimized normalized window length

As the number of zeros retained increases, the ripple of the FIR filter in frequency-domain reduces substantially; hence, the filter is closer to the infinite (IIR) filter. This study chose a time window length of 6.895.

3.2.6 Fast Displacement Estimation (FDE) through iFFT

Equation (26) shows how to compute the coefficients of the filter for defined parameters. This approach requires evaluating an integral for each point in the filter, which means $2k+1$ integrals. Matlab® has several options to evaluate numerically the integrals; using anonymous functions is a fast and robust option.

The integrals to be evaluate are the product of the function times a cosine series, which resembles an inverse Fourier transform. This research proposes to evaluate the integral in Eq. (26) using the inverse fast Fourier transform. Figure 3.11 shows the comparison of numerical integration and plain inverse FFT, which does not exhibit good results.

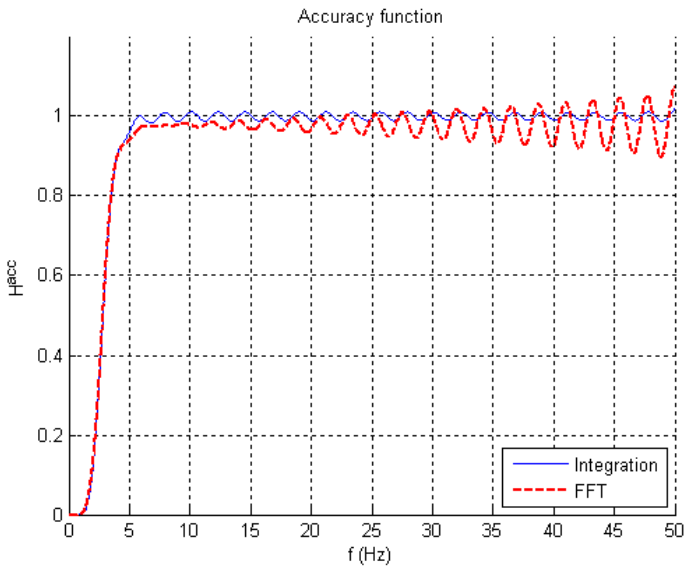

Figure 3.11 Accuracy function of filter using integration and iFFT

To improve the results of the inverse FFT, the research team proposed a new approach, termed fast displacement estimation (FDE), to compute the filter coefficients using resampling. Instead of using Eq. (27) for the number of sampling points, researchers propose Eq. (28) to obtain k_p, such that the transfer function is sampled in $2k_p+1$ points from 0 to f_s; the other parameters are the same as before. Then, an inverse FFT algorithm was applied to the sampled points in the frequency-domain to obtain the points in the time-domain. The middle $2k+1$ points correspond to the coefficients of the FIR filter, thus the length of the FIR filter remains unaltered. N_p is a positive integer called the resampling ratio, and as it increases, theoretically the accuracy will improve:

$$k_p = N_p \frac{N_w f_s}{2 f_T} \tag{28}$$

Figure 3.12 shows the results in time-domain and frequency-domain using integration and the new proposed approach with $N_p = 20$. This figure shows that the results agree well in both domains.

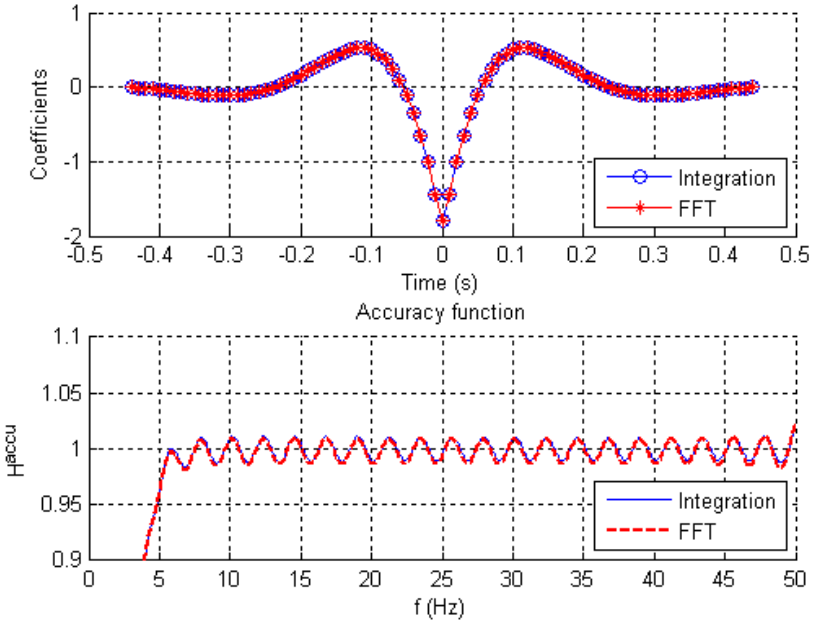

Figure 3.12 Coefficients and accuracy function of filter using integration and FDE

To assess the performance of the new approach, researchers applied the new approach for several values of N_p and measured the error in the frequency-domain and the run time of the algorithm. Figure 3.13 shows the results obtained: the first plot shows that the error decreases as N_p increases, and the second plot show that the relative time with respect to the time using integration is small. For instance, using $N_p = 20$, the RMS error is less than 0.1 percent, and the running time is less than 1 percent of the time using (numerical) integration; as a result, researchers recommend using the former value to achieve good accuracy and reduce computation time.

Furthermore, this method is particularly suitable for implementation on WSS because it requires only the coding of inverse FFT, which is readily available, to compute the coefficients of the filter. These coefficients are applied to the measured data to obtain near-real-time displacement estimates. Note that the time lag in the displacement data is half the time window of the filter, which is typically less than few seconds.

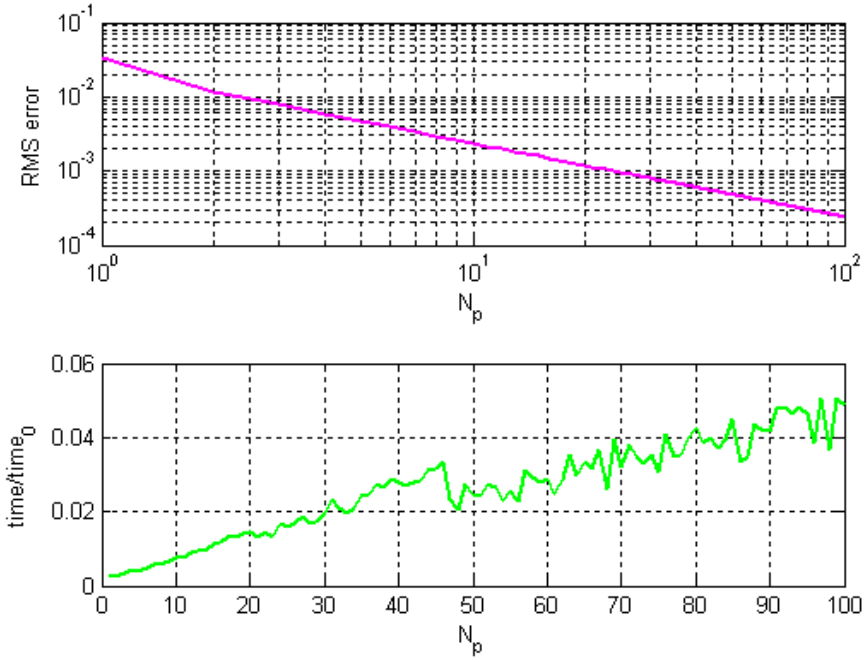

Figure 3.13 Coefficient error and time comparison of FDE with respect to integration

3.3 Validation of the Method

The following sections discuss the validation of the approach.

3.3.1 Numerical Validation

Researchers first validated the proposed method numerically, based on the field displacement records measured from the Bluford bridge with train passage at different speeds.[2] The acceleration signals were obtained though numerical differentiation; subsequently, 1 percent RMS noise was added to simulate measurement errors.

A total of 10 cases of field displacement were used for numerical validation: 5 mph SB, 5 mph NB, 10 mph SB, 10 mph NB, 15 mph SB, 15 mph NB, 20 mph SB, 20 mph NB, 25 mph SB, and 25 mph NB. (SB and NB stand for southbound and northbound.) The acceleration and displacement (see Figure 3.14) tended to be larger as the speed of a train increased.

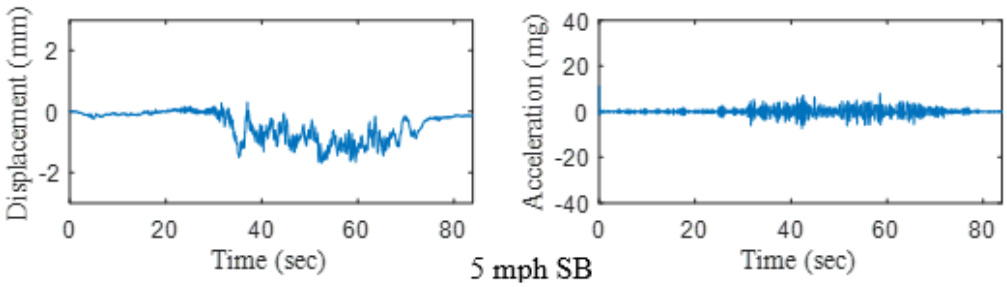

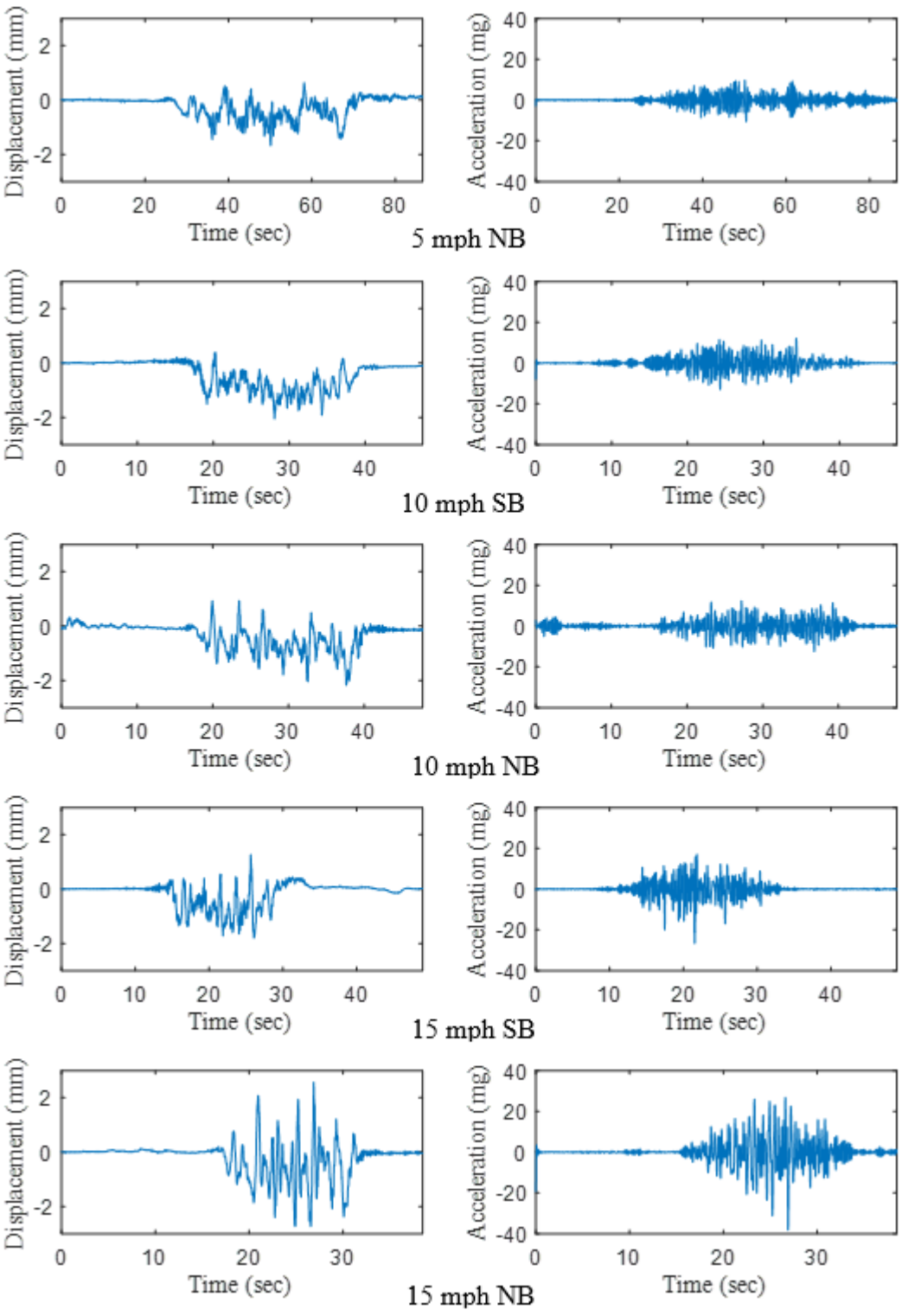
Displacement (mm)
Acceleration (mg)
Time (sec)
5 mph NB
10 mph SB
10 mph NB
15 mph SB
15 mph NB

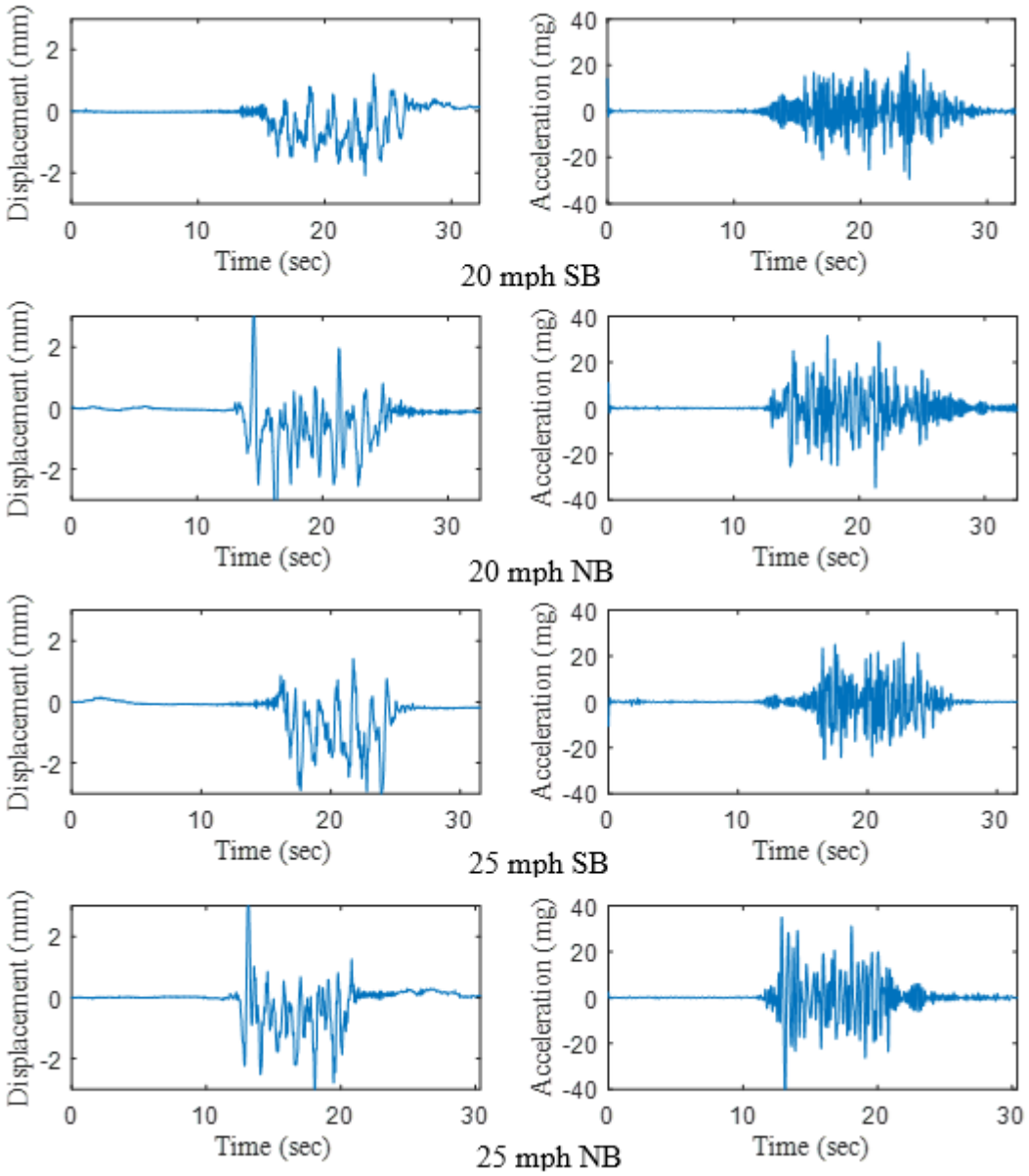

Figure 3.14 Measured displacement and derived acceleration for numerical validation in Case 1 to Case 10

As the proposed method estimates dynamic displacement using an acceleration record, measured dynamic displacement was extracted out of total displacement by applying a 0.5 Hz high-pass filter, because acceleration record below 0.5 Hz was considered a pseudo-static response. The dynamic displacement was extracted from the total displacement using this filter. At a low-speed train passage, pseudo-static displacement governs the entire displacement; at higher speeds, the dynamic displacement is the larger portion of the total displacement.

The dynamic displacements from two different methods, i.e., the method used by Moreu et al.[2] and the proposed method are compared in Figure 3.15. Researchers used the following parameters: $f_s = 100\,Hz, f_T = 0.5\,Hz, \alpha_T = 0.99, \mathrm{n} = 4, N_w = 6.895, N_p = 20$.

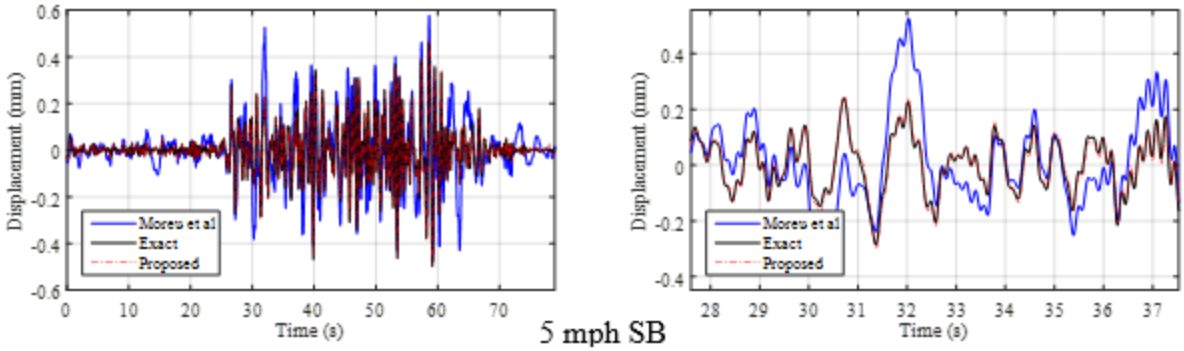

5 mph SB

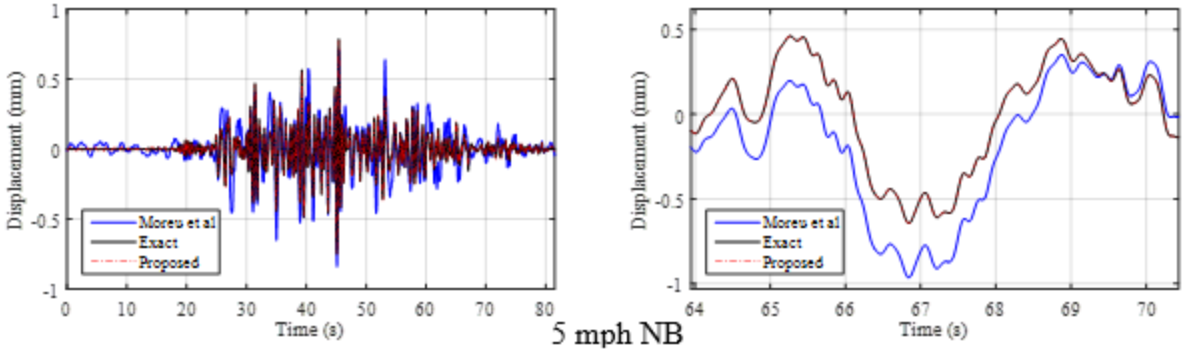

5 mph NB

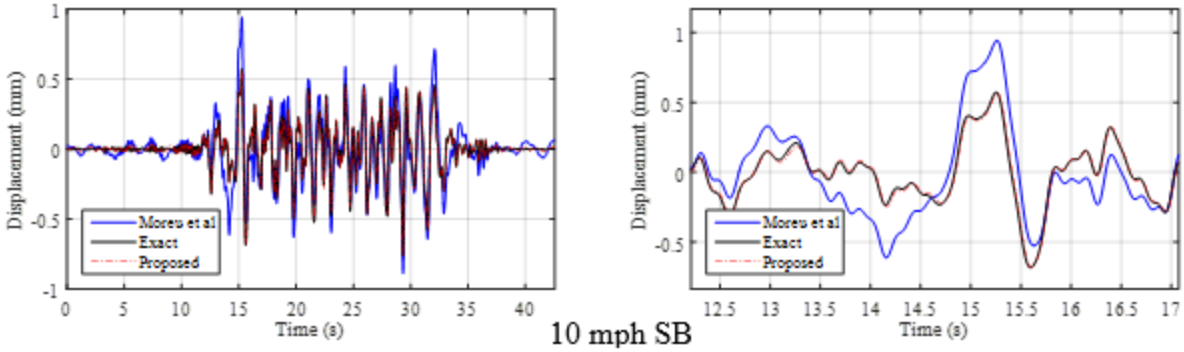

10 mph SB

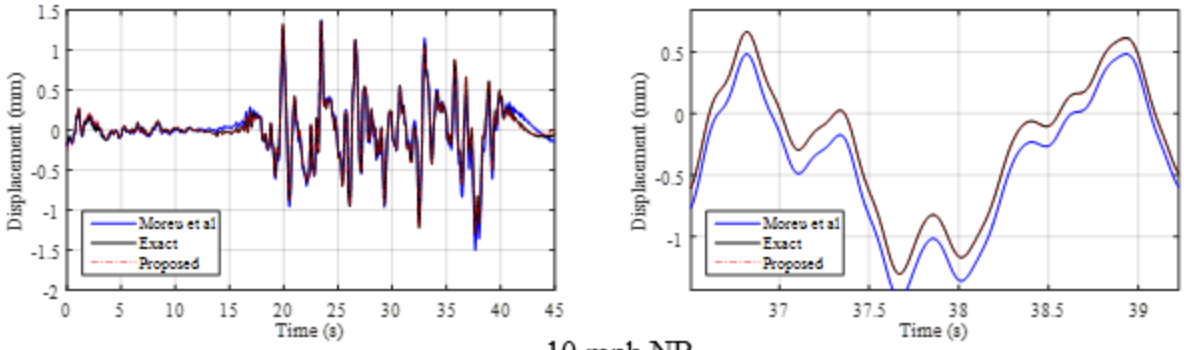

10 mph NB

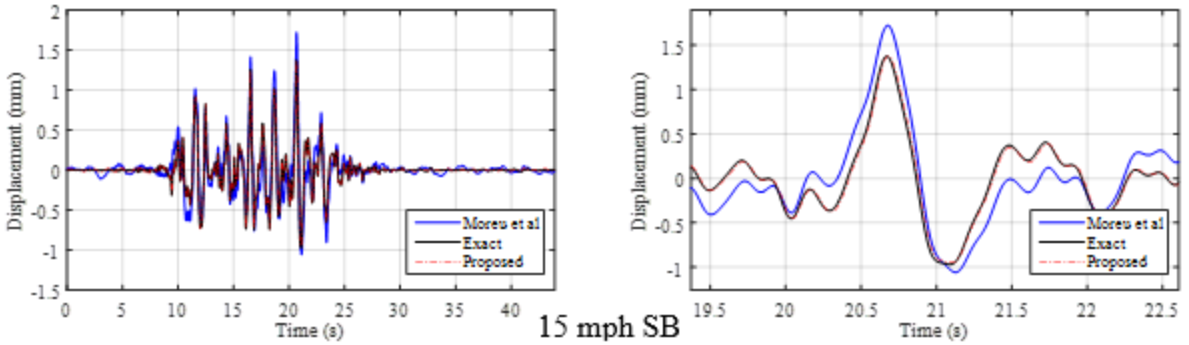

15 mph SB

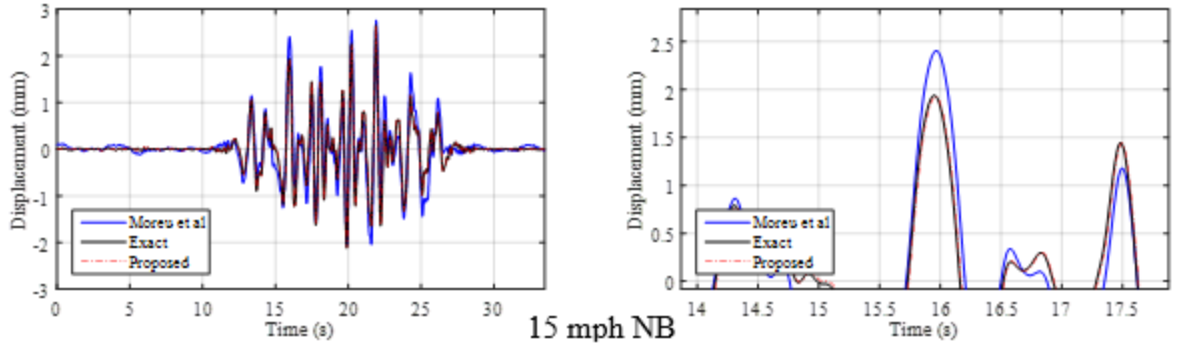

15 mph NB

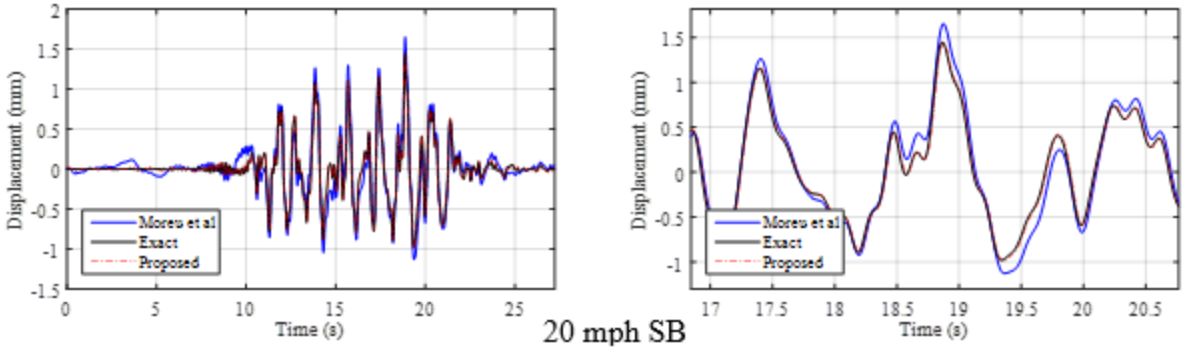

20 mph SB

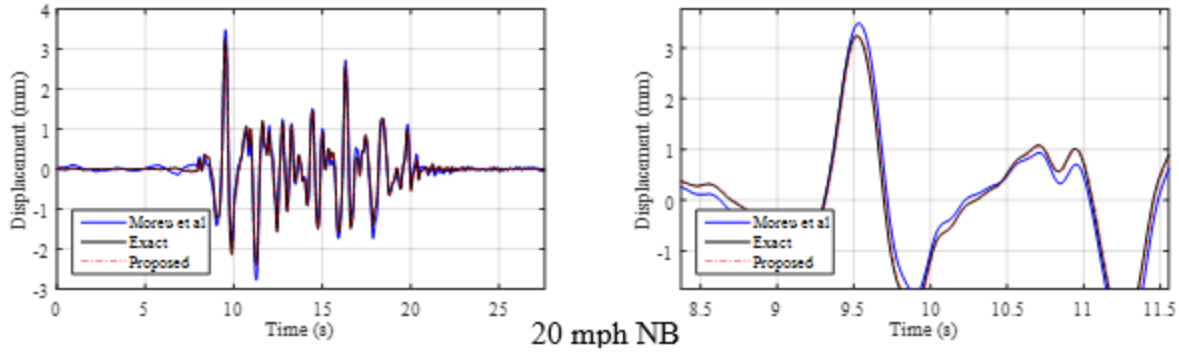

20 mph NB

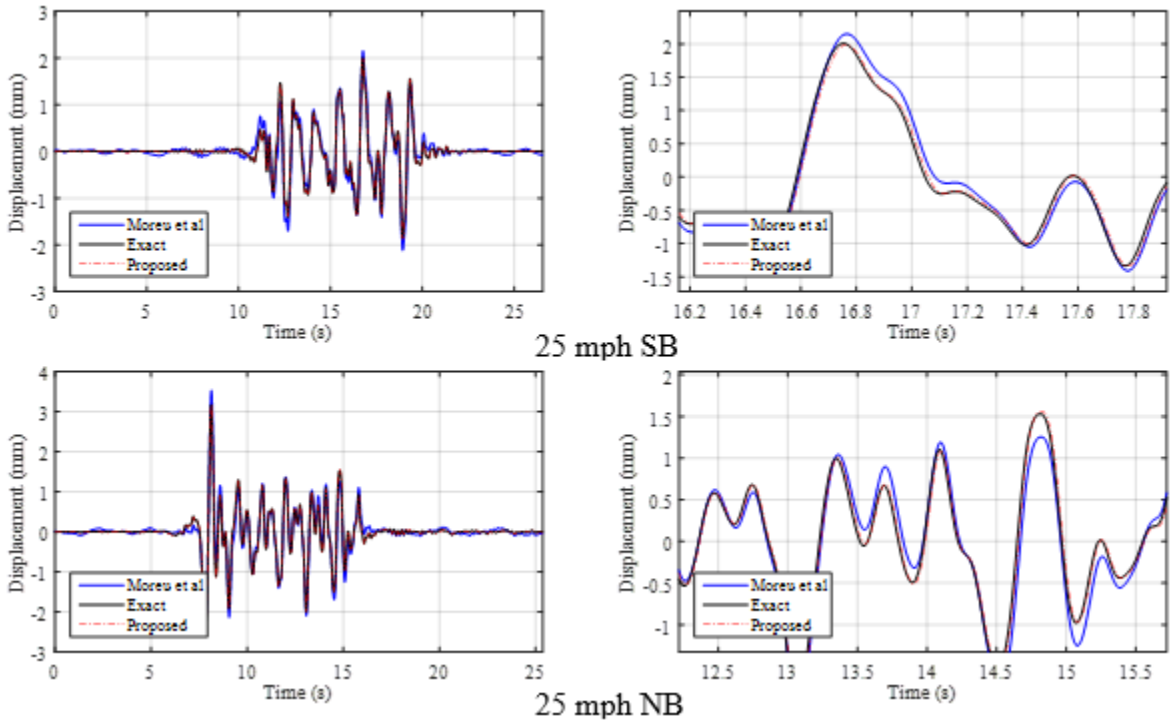

Figure 3.15 Comparison of Dynamic Displacement Estimation

To illustrate the accuracy of the results, RMS error and peak-to-peak error were defined; the RMS error can be expressed as

$$RMS\ Error = \frac{\sqrt{\sum_{k=1}^{n}(D_{Exact} - D_{Est})^2}}{\max(D_{Exact})} \tag{32}$$

where n, D_{Exact} are D_{Est} are number of data points, exact dynamic displacement, and estimation dynamic displacement. Peak-to-peak error was defined by the difference of estimated dynamic displacement from exact displacement over maximum exact dynamic displacement. The results are summarized as in Table 3.1. The previous approach showed a large variance from 3.52 percent to 18.21 percent in RMS error and 4.10 percent to 25.63 percent in peak-to-peak error, while the proposed method shows more consistency in errors, with a maximum of 3.55 percent.

Table 3.1 Error of dynamic displacement estimation

Case	RMS error (%)		Peak to Peak error (%)	
	Moreu et al. 2015	Proposed	Moreu et al. 2015	Proposed
5 mph SB	17.53	2.12	25.63	3.55
5 mph NB	11.06	1.11	9.74	0.78
10 mph SB	18.21	2.01	64.70	0.93
10 mph NB	11.39	1.09	20.36	0.61
15 mph SB	8.49	0.79	22.69	0.61
15 mph NB	7.59	0.49	4.10	0.01
20 mph SB	7.08	1.01	14.32	0.23
20 mph NB	3.79	0.37	7.58	0.53
25 mph SB	5.33	0.57	7.11	1.02
25 mph NB	3.52	0.49	11.17	0.28

3.3.2 Experimental Validation in Laboratory

The displacement measurements from these field tests were reproduced on a hydraulic motion simulator, and dynamic displacement was estimated using an accelerometer attached on the motion simulator as shown in Figure 3.16. The hydraulic motion simulator utilizes six independent actuators to allow control of the Cartesian coordinate. In the experiment, the field-measured lateral displacement of the Bluford bridge was used. The accelerometer had a sensitivity of 0.998 g/V and was connected with a Vibpilot, which is a 24-bit, high-resolution spectrum analyzer. The LVDTs embedded in each actuator were also connected with Vibpilot for easier data synchronization. The actuation and data acquisition was set to 100 Hz and 64 Hz, respectively. A validation was carried out for the same 10 cases used in the numerical validation.

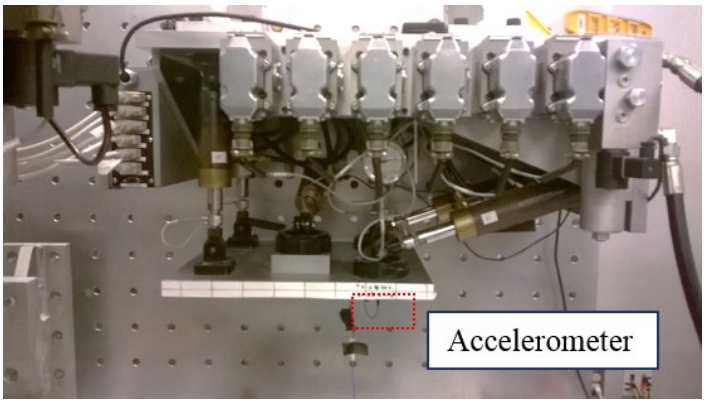

Figure 3.16 Hydraulic motion simulator and accelerometer setup

The 10 cases of displacement were reproduced by the hydraulic motion simulator. Dynamic displacement was extracted by applying a FIR high-pass filter at 0.5 Hz to eliminate pseudo-static displacement. The results are shown in Figure 3.17.

The dynamic displacement was estimated from the acceleration measurement and compared with the extracted dynamic displacement from the hydraulic motion simulator, Figure 3.18.

The result of experimental validation, as shown in Table 3.2, indicates that the proposed displacement estimation method estimates dynamic displacement very accurately, with a maximum error of 3.59 percent.

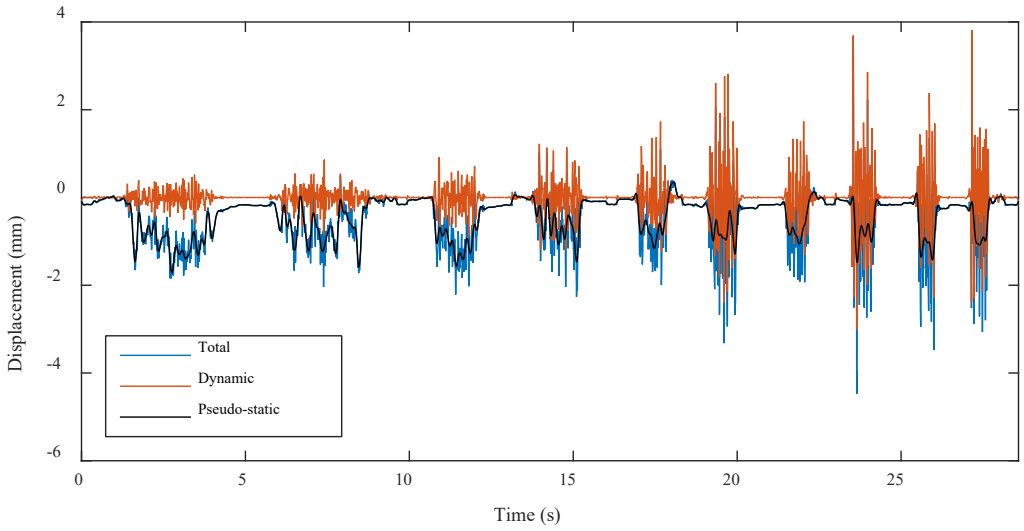

Figure 3.17 Total and dynamic displacement reproduced by a hydraulic motion simulator for the 10 cases considered

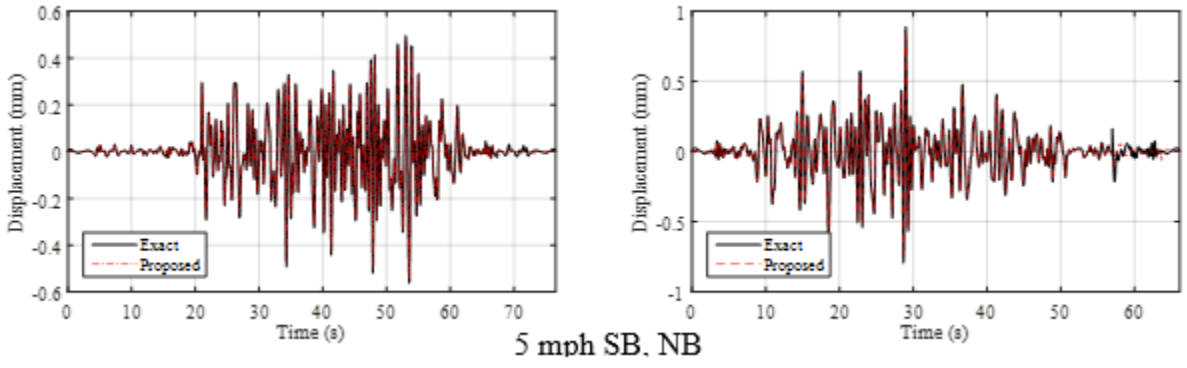

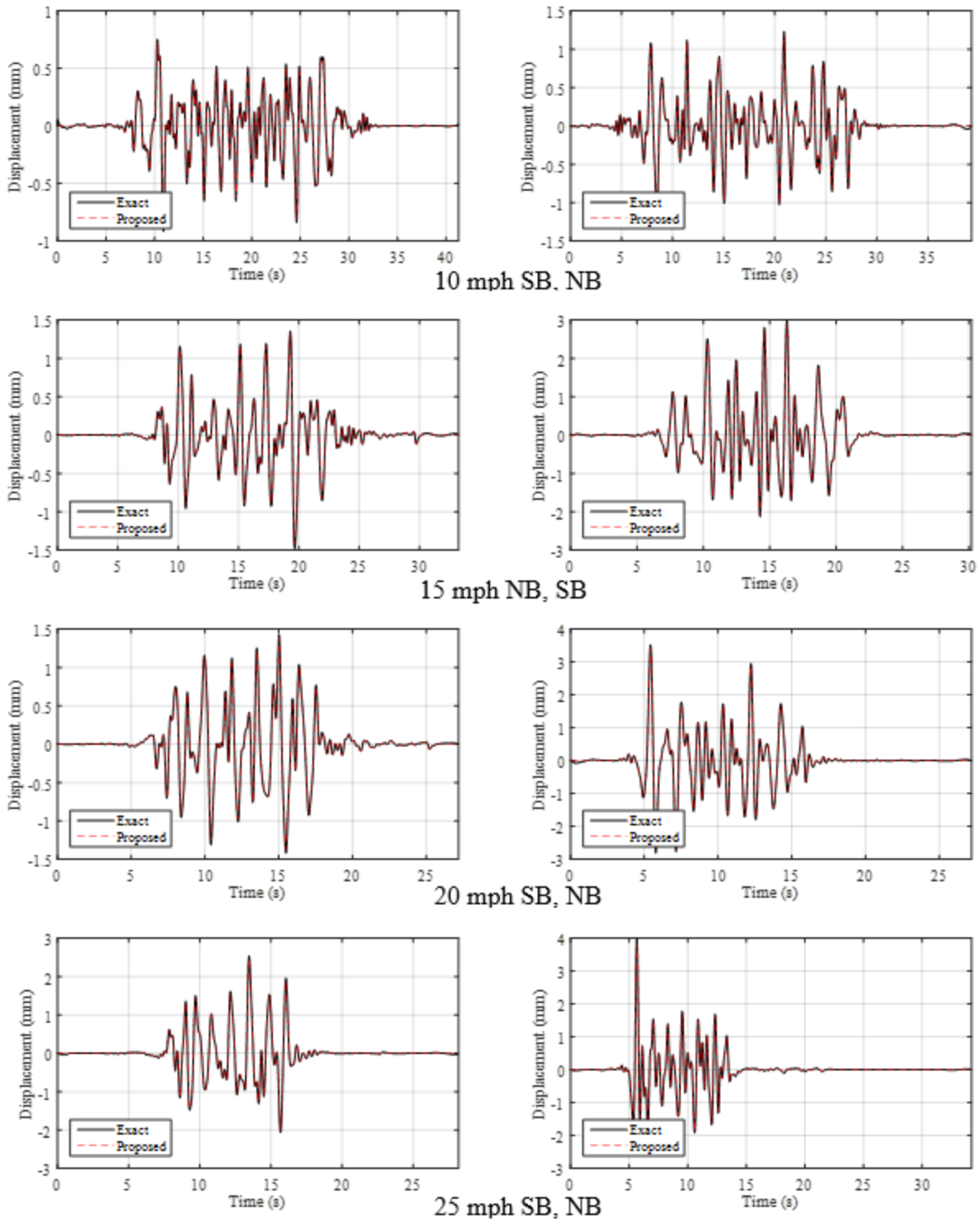

Figure 3.18 Comparison of the dynamic displacement estimation

Table 3.2 Results of the experimental validation

Trains	Peak-to-Peak Error (%)	RMS Error (%)
5 mph SB	2.75	1.35
5 mph NB	2.91	2.12
10 mph SB	3.34	1.34
10 mph NB	3.30	1.09
15 mph SB	1.70	1.00
15 mph NB	3.19	0.87
20 mph SB	1.97	1.06
20 mph NB	3.21	0.89
25 mph SB	3.25	0.89
25 mph NB	3.59	0.50

4. Bridge Selections and Descriptions

Canadian National Railway (CN) was a critical partner in this research. CN identified two timber trestle bridges and one pin-connected steel truss bridge for instrumentation and testing. CN provided access, coordination assistance, and in-kind resources for sensor installation and monitoring of this bridge. CN also provided invaluable guidance regarding issues of importance to railroad operations.

The University of Illinois research team deemed these bridges well-suited for this project for several reasons:

1) Per FRA,[9] 77 percent of North American railroad bridges are made of either steel or timber.
2) The first two bridges are approximately a quarter-mile apart, which facilitates monitoring of both bridges during a single campaign. The third bridge is easily accessible by foot.
3) One of the timber trestle bridges has been selected for replacement; thus, it served as a typical case of poor performance.

4.1 Bridge Descriptions

Two of the selected bridges are located at mileposts 78.30 and 78.00 on the CN Freeport line. Their proximity to each other allowed researchers to monitor them in a single campaign outing. Figure 4.1 shows the location of the site and the location of the University of Illinois; the bridges are located in Deer Run Forest Preserve in Cherry Valley, Illinois, which is close to Rockford. Figure 4.2 shows recent photographs of both bridges.

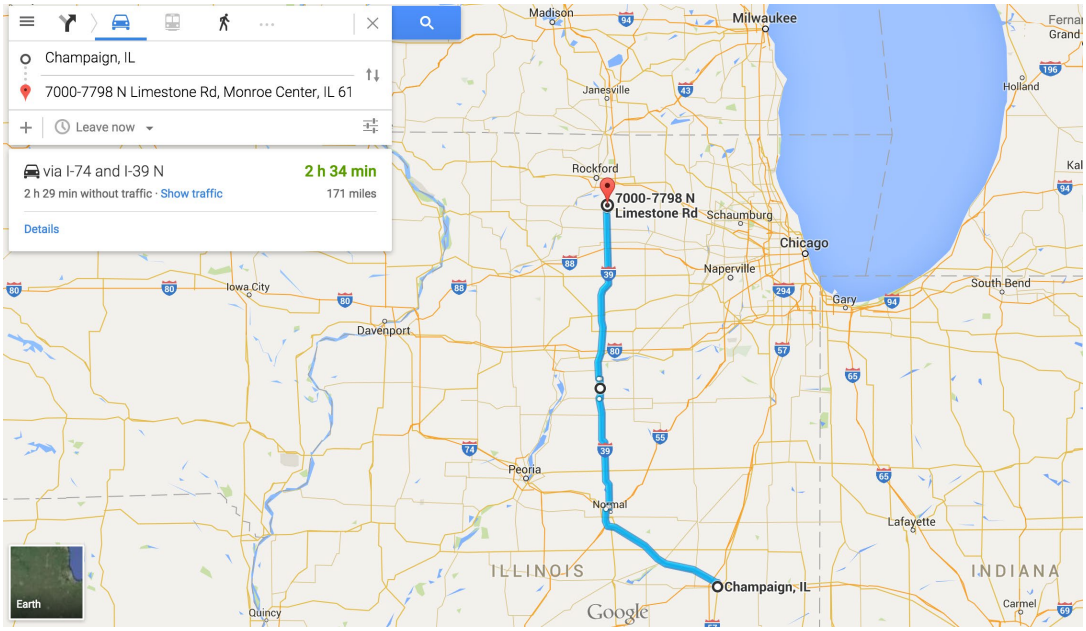

Figure 4.1 Location of the bridges Freeport 78.00 and 78.30

Figure 4.2 Bridges (a) Freeport 78.00 and (b) Freeport 78.30

The bridge on the Freeport line at milepost 78.00 (termed herein Freeport 78.00) is a timber trestle bridge composed of 13 piers and 2 abutments; the piers are spaced 12.5 to 13.5 feet apart for a total length of 182 feet. The bottom of the deck is approximately 16 feet from the mean water level. The pier consists of six, 14-inch-diameter timber piles with variable batter, supporting a timber bent cap. The bent cap carries the longitudinal stringers on which the deck planks are laid. Figure 4.3 shows an elevation view of the bridge.

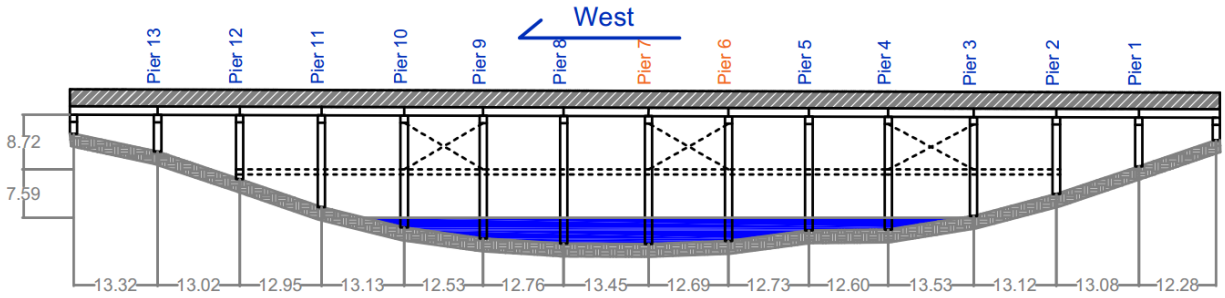

Figure 4.3 Timber trestle bridge dimensions

CN retrofitted this bridge with additional X-bracing in the longitudinal and lateral directions. Due to settlement of some piles, they placed shims on the top of the pile to ensure contact of the bent cap with the piles.

Freeport 78.30 is a pin-connected steel truss bridge composed of two 150-foot trusses for a total length of 300 feet. In each truss, the top chord is composed of built-up sections. The bottom chord is composed of built-up sections and pin-eye bars. The vertical elements are built-up sections and the diagonals are pin-eye bars. Built-up transverse beams connect the nodes in the top chord, which provides lateral stiffness to the system. Each node of the bottom chord supports a transverse plate girder, which carries longitudinal stringers supporting the deck. Figure 4.4 shows an elevation of the bridge in the longitudinal direction.

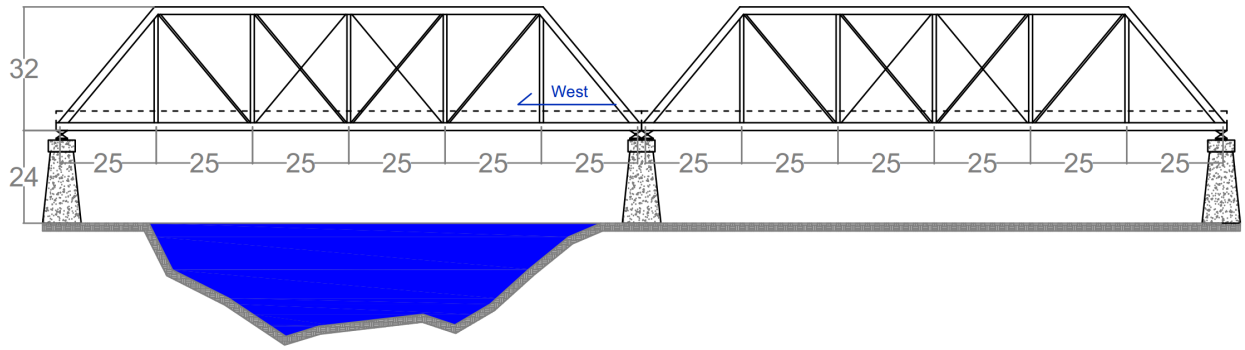

Figure 4.4 Pin-connected steel truss bridge dimensions

In addition, each truss is stiffened with X-bracing in the top and bottom chords. CN replaced the X bracing in the bottom chords with similar sections and added some additional bracing. Figure 4.5 shows the details of the additional Chevron bracing composed of I-beams; this bracing stiffens the truss longitudinally and laterally.

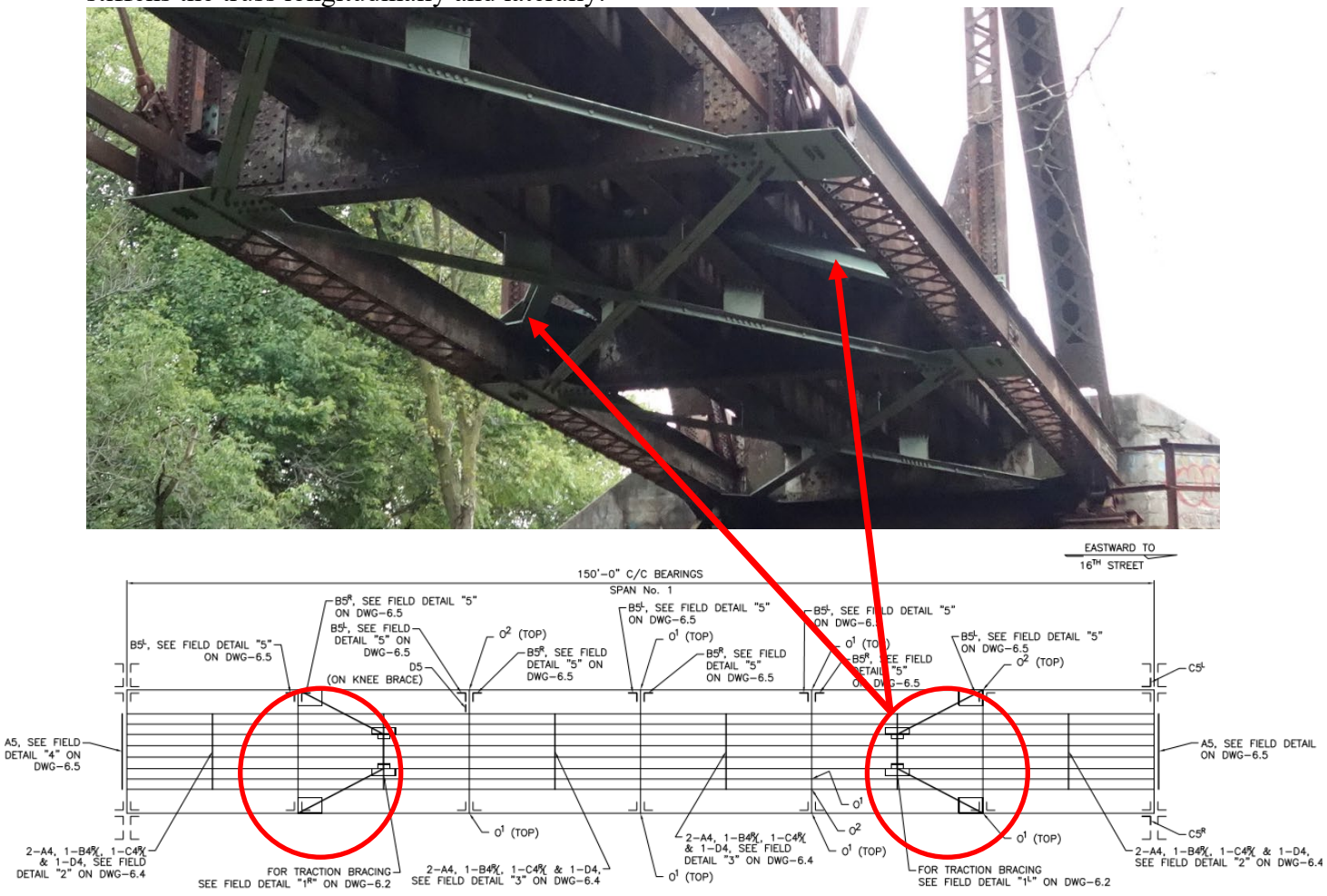

Figure 4.5 New bracing added during repairs

The researchers worked with a third bridge, Freeport 33.00, to perform supplementary field tests. This bridge is easily accessible, and other researchers have monitored this bridge to measure lateral displacement using a laser-based approach.[2] Freeport 33.00 is a combination of timber piers on the approaches and steel plate girder in the main span over the highway. The piers monitored consist of six 14-inch-diameter timber piles with variable batter, which support a concrete bent cap. The bent cap supports longitudinal stringers, and these support the deck planks. Figure 4.6 shows a photograph of the bridge. All of these bridges are in service with freight traffic – usually 2 trains per day for Freeport 78.00 and 78.30 and fewer than 10 trains per day for Freeport 33.00.

Figure 4.6 Freeport 33.00

5. Preliminary Bridge Monitoring Campaign

This section presents the details and tests conducted in a preliminary monitoring campaign. Specifically, this section describes the use of a vision-based displacement measurement method that was used as a reference for the new accelerometer-based method.

5.1 Camera-based Displacement Estimation

Researchers used a computer-vision-based method proposed by Yoon et al.[21] The computer-vision-based method was comprised of: (1) camera calibration, (2) natural feature detection, and (3) feature tracking. Figure 5.1 shows the computer-vision framework.

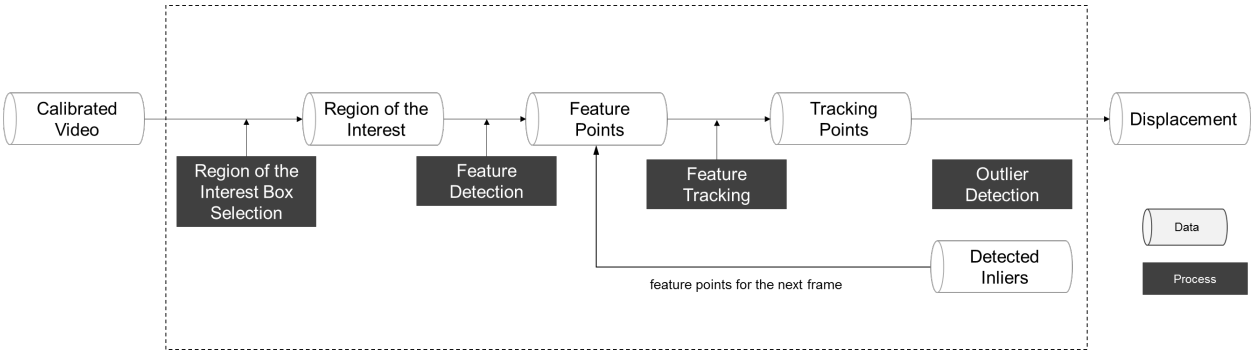

Figure 5.1 Camera-based displacement estimation framework

The first step in the approach is camera calibration. Modern consumer-grade cameras have improved dramatically in recent years, but often employ very wide-angle lenses. They increase the field-of-view by intentionally introducing radial distortion. To remove this distortion and get accurate displacement measurements using consumer-grade cameras, performing camera calibration is necessary. The process determines the pixel scaling factor, camera focal length, lens axis offset, and the lens distortion characteristics. Displacement measurements are extracted from the calibrated video images. UIUC used the camera calibration method reported by Zhang[22] in this project.

After calibration, the dynamic response of structures is determined by analyzing the video frame-by-frame. To achieve reliable tracking, distinct features are selected on the object of interest. These features should be invariant to changes in illumination, scale, and pose. Several feature detection methods exist. In this project, the corner detection method suggested by Harris and Stephens[23] was used to extract the features in the initial video frame. Figure 5.2 shows example feature points detected from the truss bridge using the corner detection method.

---

[21] Yoon, H., Elanwar, H., Choi, H., Golparvar-Fard, M., & Spencer, B.F. (2016). Target-free Approach for Vision-based Structural System Identification using Consumer-grade Cameras. Structural Control and Health Monitoring, DOI:10.1002/stc.1850.

[22] Zhang, Z.Y. (2000). A flexible new technique for camera calibration. IEEE Transactions on Pattern Analysis and Machine Intelligence, **22**(11): p. 1330-1334.

[23] Harris, C., & Stephens M. (1988). A combined corner and edge detector in Alvey vision conference. Manchester, UK.

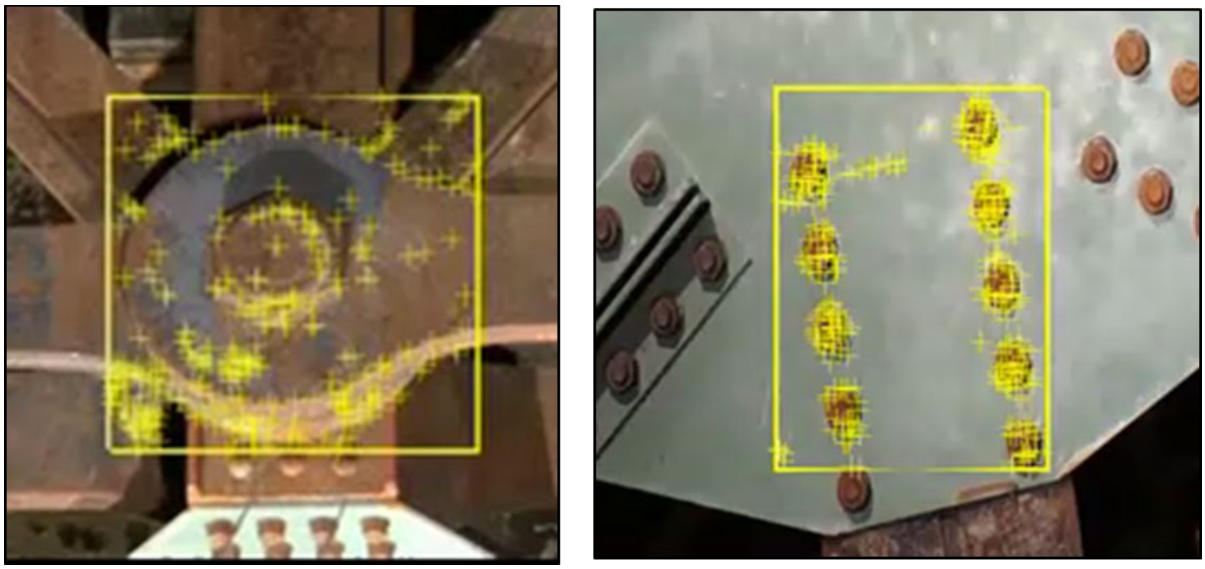

Figure 5.2 Natural feature detection examples

Once the features were selected for the initial frame, the optical flow method suggested by Lucas and Kanade[24] were used to track the point features for the entire duration of a video. Finally, homography and outlier removal algorithms were employed to obtain sub-pixel accuracy in the displacement measurement.

5.2 Preliminary Measurements and Results

For the final monitoring campaign, researchers visited the site twice. The first preliminary test was on September 18, 2015. The goal of the test was to evaluate the general conditions of the site and to do a preliminary assessment of the camera system. The measurements in this visit were not satisfactory due to several factors, but they served to improve the measurement methods for next tests.

The second visit was on October 28, 2015. The goal of the test was to measure displacements of the steel truss bridge using video cameras with a more robust setup. Figure 5.3 shows the researchers installing the equipment. The train passed by the bridges at night; therefore, the researchers installed halogen lamps to improve the lighting for the points of interest. The researchers did not place targets on the bridge because they were not allowed to foul the track. The measurements relied on the extraction of information from the natural features of the structure.

[24] Lucas, B.D., & Kanade, T. (1981). An iterative image registration technique with an application to stereo vision. In *IJCAI*.

Figure 5.3 Camera and halogen lights in preliminary field test

In this second visit, researchers placed three cameras on tripods at locations far from the abutments to avoid soil movement. Two cameras were placed to measure displacements in the longitudinal-vertical plane, and the remaining camera was placed under the bridge to measure displacements in the longitudinal-transversal plane. Using the vision-based method researchers estimated displacements in the three main directions. Figure 5.4 shows the displacements in the three main directions obtained after processing the videos.

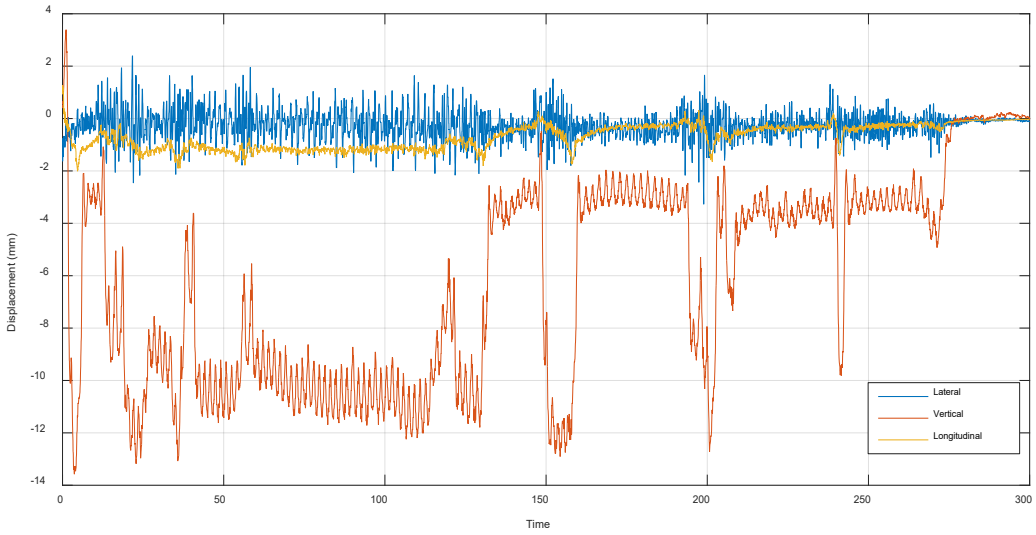

Figure 5.4 Displacement estimation in 3 directions from vision-based method

The measured displacements were consistent with the results obtained in the previous campaign monitoring of pin-connected trusses.[25] Vertical displacement of the bridge was controlled by pseudo-static displacement from the direct application of the loads. To assess the frequency components of the displacements, researchers computed the power spectral density (PSD) of the signals, shown in Figure 5.5. This figure displays the beating frequency of the train, 0.56 Hz, which was consistent with the 30-mph speed of the train. In the lateral direction, there were important components over a broader range of low frequencies; meanwhile, in the vertical direction, the important frequency components were near the zero frequency, which represents the pseudo-static displacements.

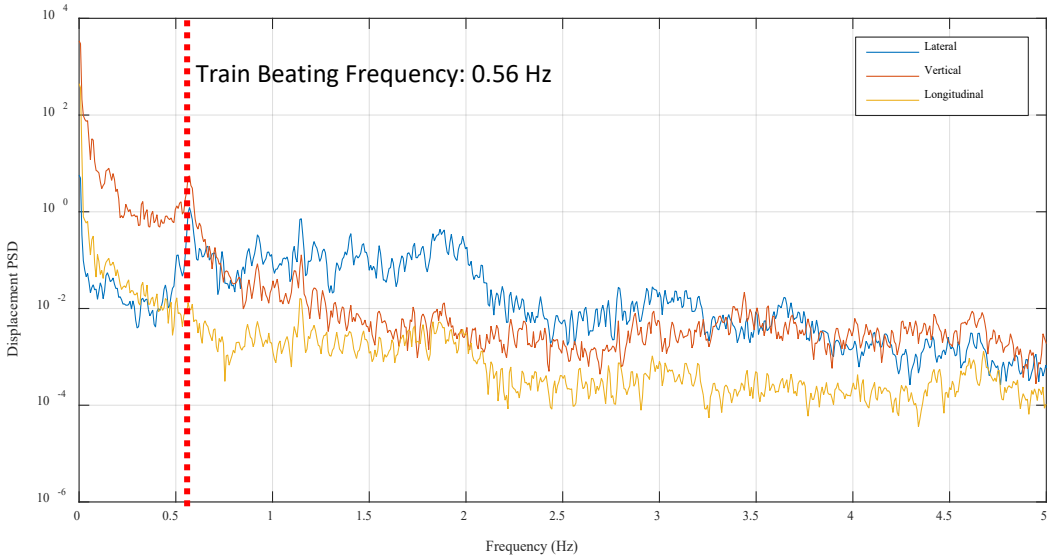

Figure 5.5 PSD of displacements

To compare the accuracy of the vision-based methods, researchers built a finite element (FE) model of the bridge under train loading to estimate vertical displacements. CN provided drawings of the bridge and the train manifest with the weights of the cars, from which researchers estimated wheel loads and train mass. The FE model considered train loads as concentrated moving loads, and it also included the additional mass of the train as concentrated moving masses. Then, the second-order equations of motion were converted to a first-order system, also known as the state-space representation. Since the mass varies in time, a special block was built in Simulink to account the change in the mass matrix. Researchers used Simulink to solve the first-order system in time for the train loading. They used additional blocks to model a DAQ system with an anti-aliasing filter to simulate field data.

[25] Moreu, M., Altwood, T. J., Jo, H., Kim, R., Cho, S.,LaFave, J.M., and Spencer Jr., B.F. (2016). Displacements of Steel Railroad Bridges under Revenue Service Traffic for Performance-Based Assessment, Proceedings of the AREMA Annual Conference and Exposition, Orlando, FL, August 27-29.

Finally, Figure 5.6 shows the vertical displacement obtained in the FE simulation together with the estimation using the vision-based method. The agreement in shape and magnitude is clear, indicating that the results from the method were reliable. Note that the delay of the signal toward the end was due to the train not having a constant speed across the bridge.

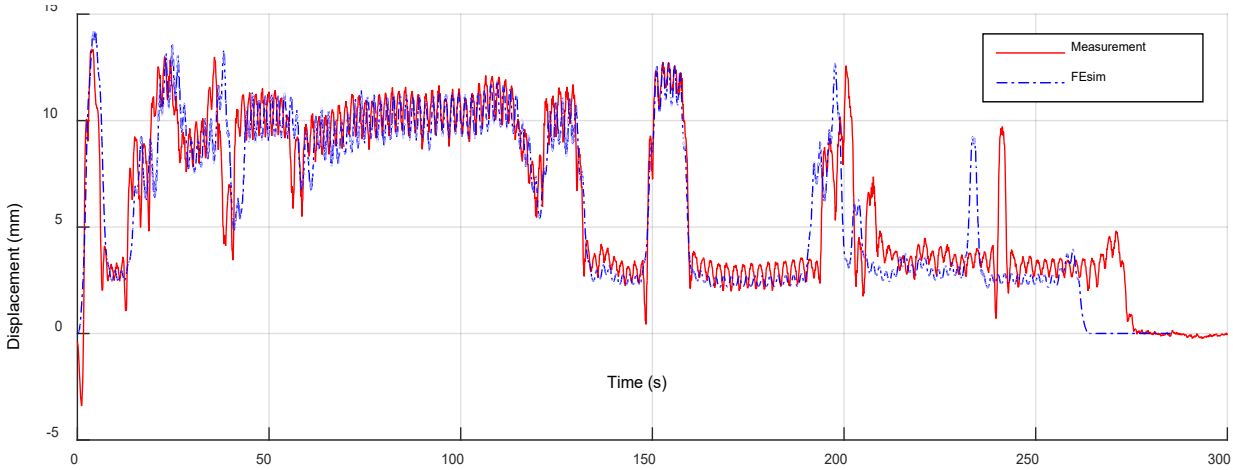

Figure 5.6 Vision-based and FE vertical displacement comparison

6. Monitoring Campaign of Bridges on CN Freeport Line

This section describes the tests of the reference-free displacement measurement technique. The timber trestle bridge, Freeport 78.00, and the steel truss bridge, Freeport 78.30, were monitored simultaneously under train revenue traffic. In addition, timber trestle bridge Freeport 33.00 was monitored separately.

6.1 Timber Trestle Bridge Freeport 78.00

Researchers instrumented the timber trestle bridge Freeport 78.00 on February 26, 2016 to obtain accelerations in the vertical and lateral directions under two trains. Reference displacements were collected using the vision-based method. The first train (primarily empty cars) passed at around 8:00 p.m. heading west, and the second train (loaded cars) passed at around 10:00 p.m. heading east.

6.1.1 Experimental Setup

Figure 6.1 shows a sketch of the experimental setup on the Freeport 78.00 bridge. Researchers used four accelerometers placed on piers 6 and 7 in each of the vertical and transverse directions to obtain the accelerations of the structure. In addition, researchers used two cameras to measure displacements, one per pier.

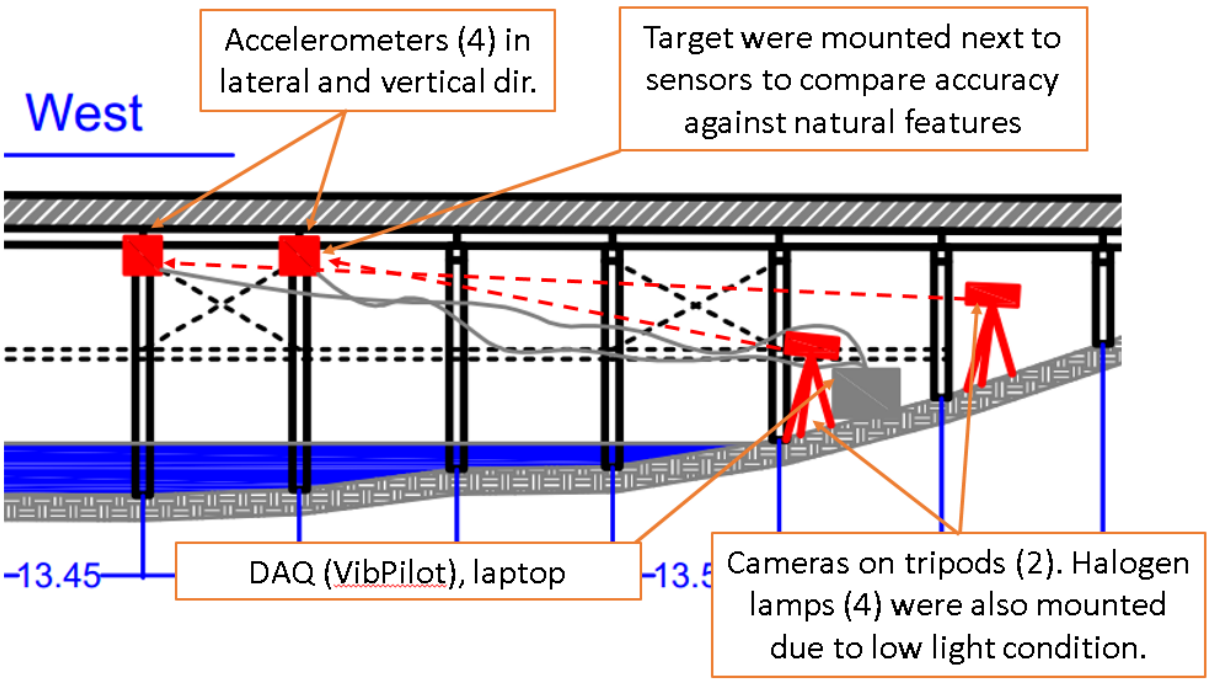

Figure 6.1 Timber trestle bridge setup

Researchers used VibPilot, a 24-bit DAQ system, to acquire data from the accelerometers. For the first train, the data was sampled at 4,096 Hz, and for the second train, the data was sampled at 128 Hz. The cameras sampled data at 60 frames per second.

Due to the water underneath the bridge, researchers built a temporary platform under the bridge using wood planks. Figure 6.2 shows the platform during the field tests.

Figure 6.2 Platform built to mount equipment

Vision-based methods can use natural features to track displacements. In this case, researchers used targets to compare the accuracy of the method with and without targets. Figure 6.3 shows the locations of the targets in both piers.

(a) **(b)**

Figure 6.3 Sensors and target at (a) pier 7 and (b) pier 6

Additional lighting was required to improve the quality of nighttime video recordings. Researchers used four halogen lamps, two per pier, to illuminate the spots. Figure 6.4 shows the locations of the cameras and the halogen lamps. The cameras were located close to the embankment. The researchers tested soil movement in this area and found that it had a negligible effect on the camera measurements.

Figure 6.4 Cameras and lights setup

6.1.2 Data Processing

Figure 6.5 shows the raw data from accelerometers for both trains. Most of the important frequency content of the measured signal is in the low frequencies. The results were decimated to a sampling frequency of 128 Hz. Figure 6.6 and Figure 6.7 show the time histories and PSDs of the accelerations for Trains 1 and 2, respectively.

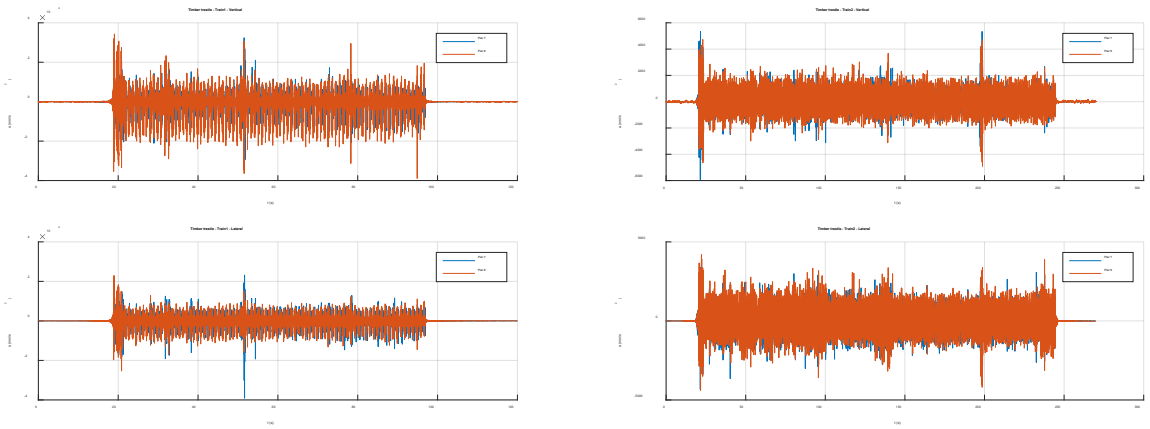

(a) **(b)**

Figure 6.5 Raw accelerations in vertical and lateral direction for (a) Train 1 (b) Train 2

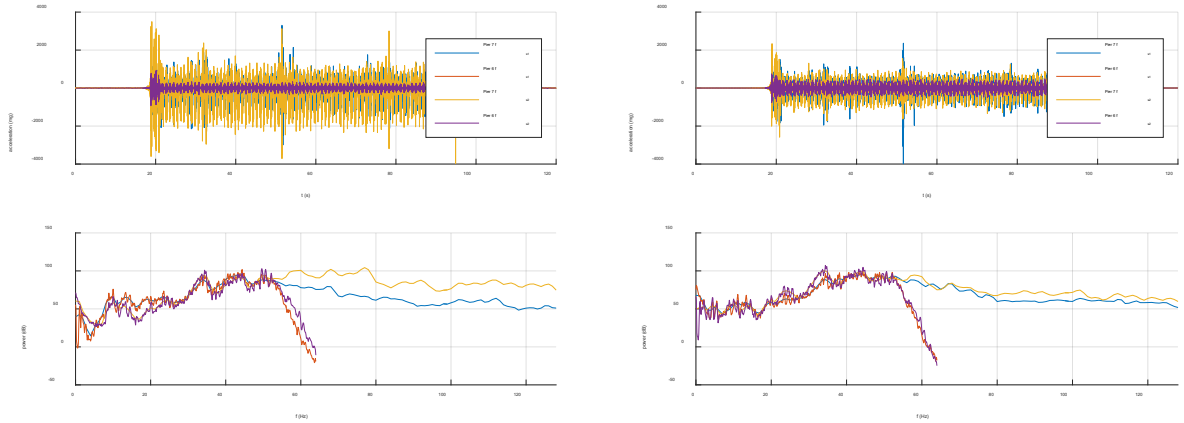

(a) **(b)**

Figure 6.6 Accelerations time-history and PSD for Train 1 in (a) vertical and (b) lateral

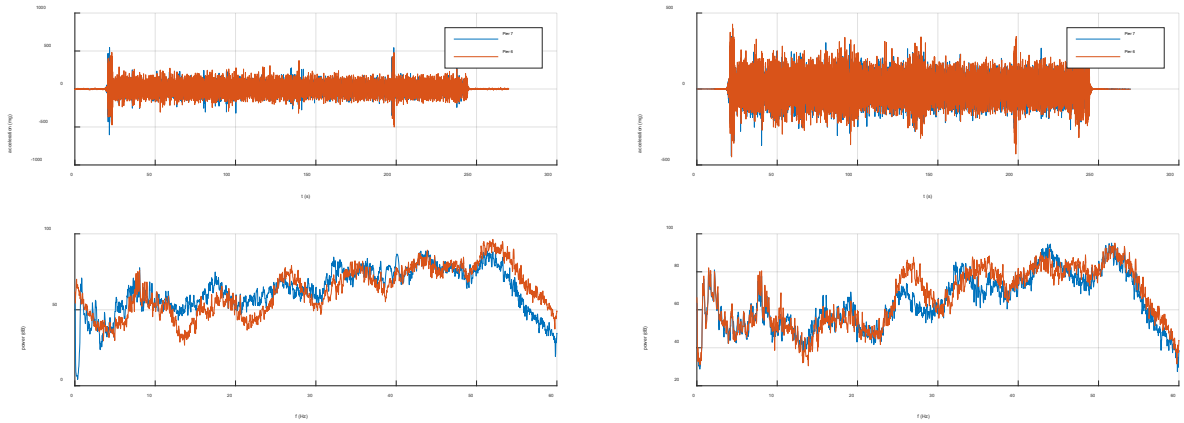

(a) **(b)**

Figure 6.7 Accelerations time-history and PSD for Train 2 in (a) vertical and (b) lateral

6.1.3 Results Comparison

To assess the adequacy of the data, the PSD of the camera-based displacement signal was obtained. In addition, researchers obtained the PSD of the acceleration signal and then applied a perfect double integrator and the FRF of the proposed continuous filter – both in the frequency-domain. Figure 6.8 and Figure 6.9 show the results for vertical and lateral directions, respectively; also, they show the PSD of the estimated displacement using FDE. Consistent data should have agreed well for frequencies larger the target frequency.

In the vertical direction, the displacement PSD results did not match well. Researchers believe this occurred because of the difficulty installing sensors in the vertical direction. Also note that for the vertical displacement, the important frequency content was located in the lower frequencies, which means that most of the displacement was pseudo-static. In the lateral direction, the displacement PSD results matched well.

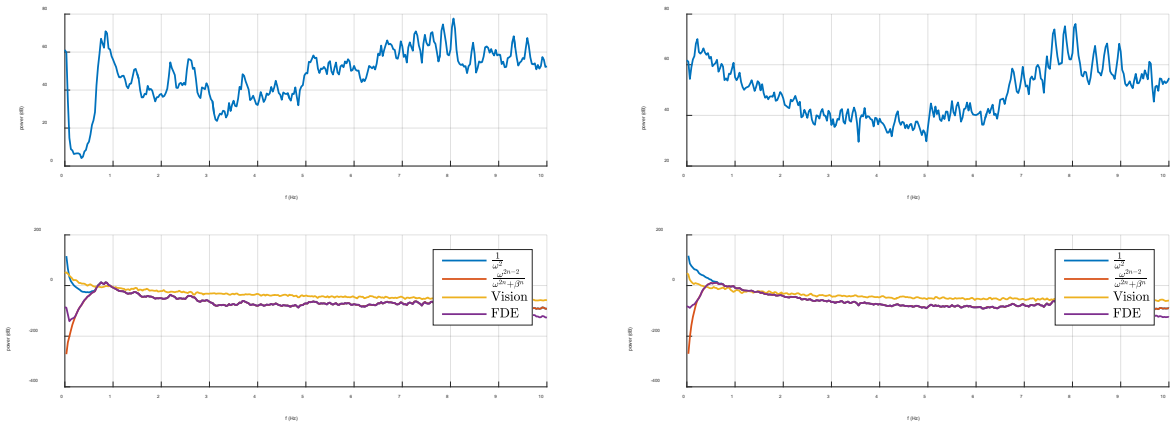

(a) **(b)**

Figure 6.8 PSD of accelerations and displacements (a) pier 7 and (b) pier 6 – vertical

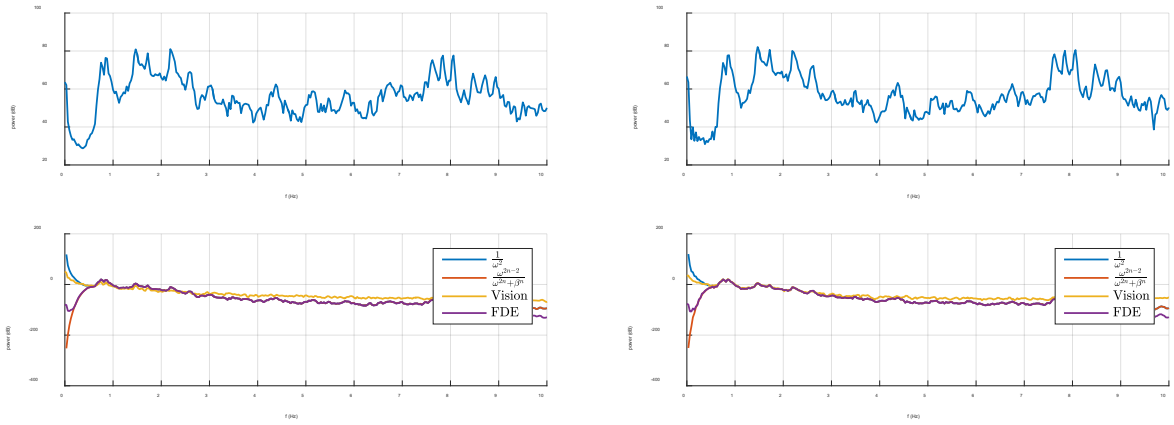

(a) **(b)**

Figure 6.9 PSD of accelerations and displacements (a) pier 7 and (b) pier 6 – lateral

The researchers extracted the dynamic displacement from vision data using traditional high-pass Butterworth filters. Figure 6.10 shows the total and dynamic displacements for lateral direction.

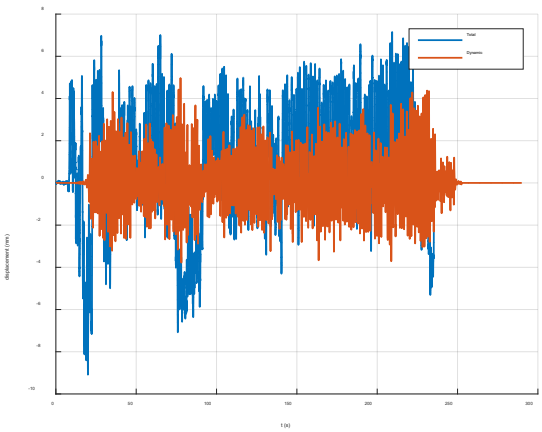

Figure 6.10 Dynamic displacement vs. total displacement for lateral direction

Finally, the researchers applied the proposed algorithm to the accelerations in the lateral direction with parameters explained in Section 4. Figure 6.12 shows the results for lateral direction in pier 6. The results matched well, as shown in the right figure, for both magnitude and phase. The peak-to-peak error was less than 1 percent, and the RMS error, as defined in Section 3, was approximately 1.6 percent. The results from pier 6 and pier 7 matched well up to a phase delay due to their spatial location.

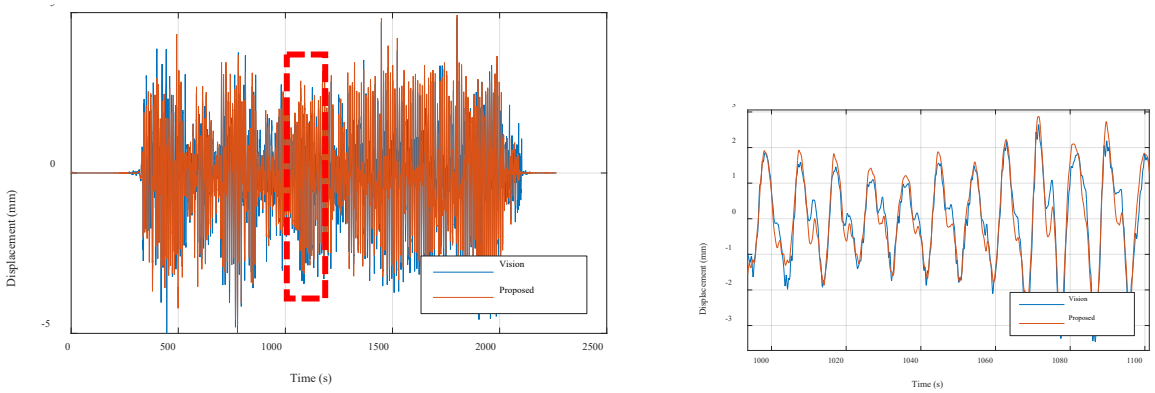

Figure 6.11 Dynamic displacement comparison in lateral direction for pier 6

6.2 Pin-connected Steel Truss Bridge Freeport 78.30

Figure 6.12 shows a diagram of the experimental setup on the timber trestle bridge. Researchers used one vertical accelerometer and one transversal accelerometer placed at the midpoint of the bottom chord. In addition, researchers used two cameras to measure displacements, one for the vertical and one for the lateral.

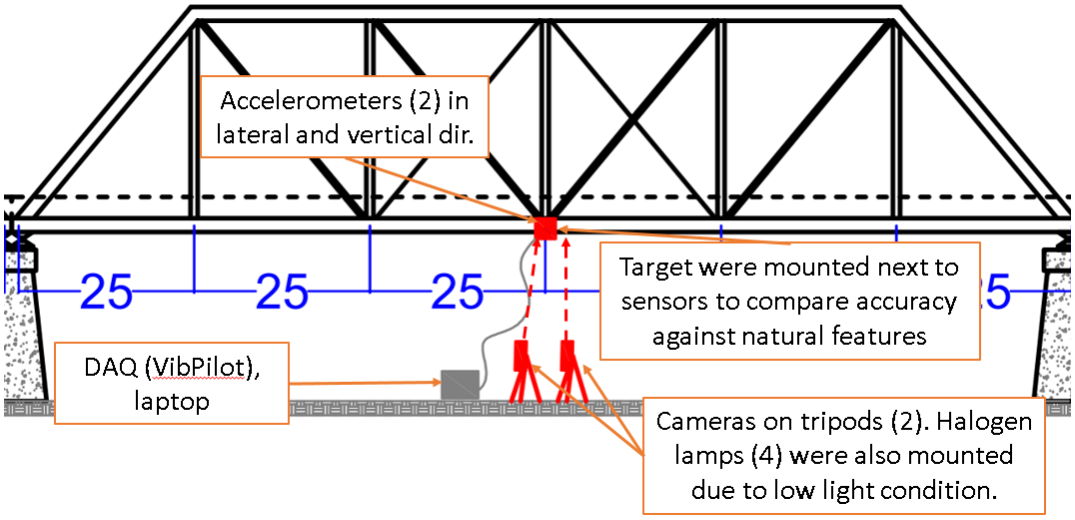

Figure 6.12 Pin-connected steel truss bridge setup

The researchers used VibPilot, a 24-bit DAQ system, to acquire data from the accelerometers. For both trains, the data was sampled at 4,096 Hz.

Due to the height of the bridge, the researchers had to use a boom lift truck. Figure 6.13 shows pictures of the researchers mounting the equipment.

Figure 6.13 Mounting of equipment

Vision-based methods can use natural features to track displacements. In this case, the researchers used a target to compare accuracy of the methods with and without targets. Figure 6.14 shows the locations of the targets. This figure also shows the sensor locations.

(a)

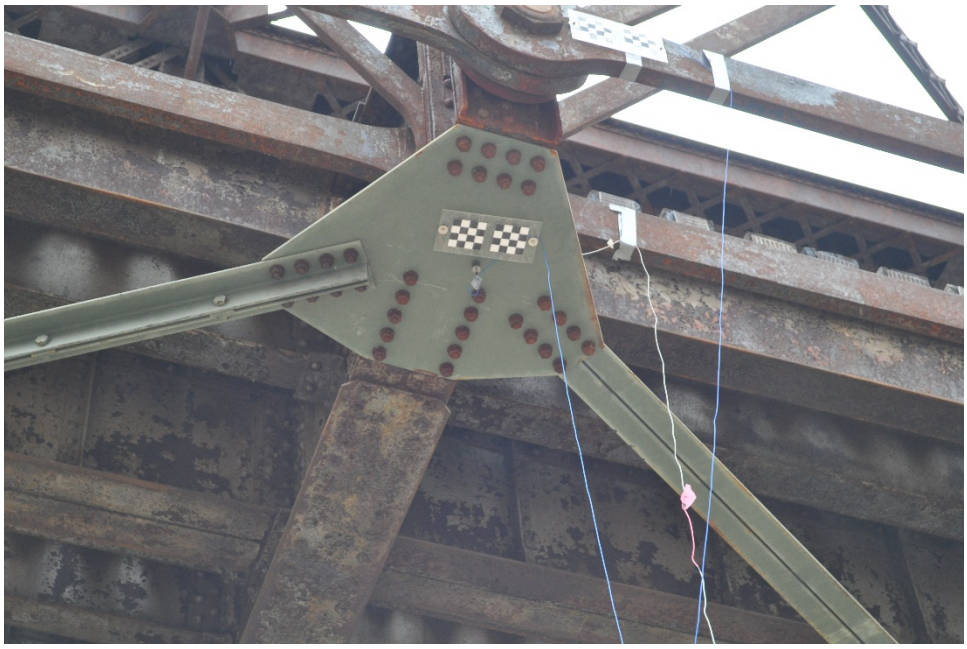

(b)

Figure 6.14 (a) Sensors and (b) targets mounted

Additional lighting was required to improve the quality of nighttime video recordings. Researchers used four halogen lamps, two for each pier, to illuminate the targets. Figure 6.15 shows the locations of the cameras and the halogen lamps. The cameras were located far from the abutments to minimize soil movement effects on the measurement.

(a) **(b)**

Figure 6.15 (a) Camera and (b) lights setup

6.2.1 Data Processing

Figure 6.16 shows the raw data from accelerometers in an actual physical unit for train 2. The results for the first unloaded train were inconsistent with measurements of other trains, and thereafter they were not considered. The most important content of the measured signal was within the low frequencies. The results were decimated to a sampling frequency of 128 Hz.

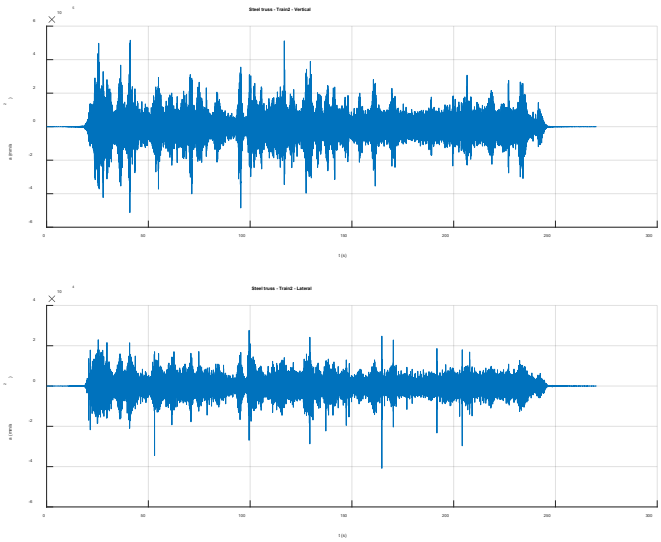

Figure 6.16 Raw accelerations in vertical and lateral directions under Train 2

6.2.2 Results Comparison

To assess the adequacy of the data, the PSD of the displacement signal was obtained. In addition, researchers obtained the PSD of the acceleration signal, and then they applied a perfect double integrator and the FRF of the proposed continuous filter – both in the frequency-domain. Figure 6.17 shows the results for vertical and lateral directions; it also shows the PSD of the estimated displacement using FDE. Consistent data should have agreed well for frequencies larger the target frequency.

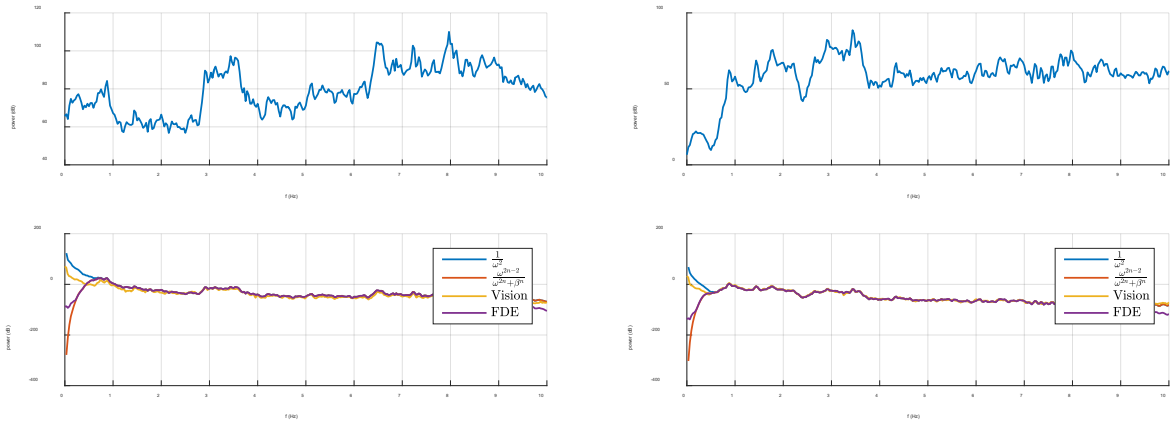

(a) **(b)**

Figure 6.17 PSD of accelerations and displacements for (a) vertical and (b) lateral

In the vertical direction, the displacement PSD results did not match well. The researchers attribute this to the difficulty of installing sensors in the vertical direction. Also note that for the vertical displacement, the important frequency content was located in the lower frequencies, which means that most of the displacement was pseudo-static. In the lateral direction, the displacement PSD results matched well.

The reference-free method estimates dynamic displacement; therefore, researchers extracted dynamic displacement from vision data using traditional high-pass Butterworth filters. Figure 6.18 shows the total and dynamic displacements for lateral direction.

Finally, researchers applied the proposed algorithm to the accelerations in the lateral direction with the parameters explained in Section 4. Figure 6.19 shows the results for the lateral direction. The results matched well, as shown in the right figure, for both magnitude and phase. The peak-to-peak error was less than 3 percent, and the RMS error, as defined in Section 3, was approximately 2.1 percent.

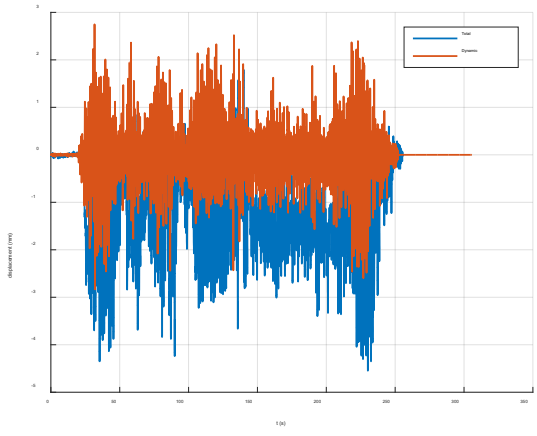

Figure 6.18 Dynamic displacement vs. total displacement for lateral direction

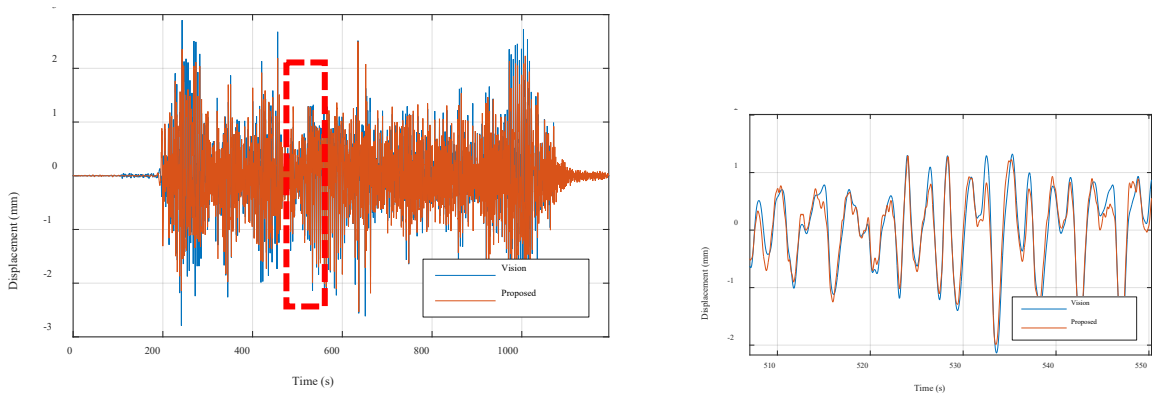

Figure 6.19 Dynamic displacement comparison in lateral direction

6.3 Timber Trestle Bridge Freeport 33.00

Researchers instrumented the Freeport 33.00 timber trestle bridge on May 23, 2016 to study the errors in vertical acceleration data from Freeport 78.0 and 78.3. This bridge was chosen because no special equipment was required to access the bridge. Data from the Freeport 33.0 bridge was used to validate the proposed method for vertical direction displacements. The train passed around 4 pm heading west.

6.3.1 Experimental Setup

Figure 6.20 shows the experimental setup on the timber trestle bridge. To understand the most important features of the vertical accelerations of the structure, four accelerometers with different characteristics were installed on the pier. In addition, researchers installed a video camera to measure displacements using targets mounted to the bridge.

Figure 6.20 Timber trestle bridge setup

The researchers used VibPilot, a 24-bit DAQ system, to acquire the data from the accelerometers; the data was sampled at 128 Hz. The cameras sampled data at 30 fps.

Figure 6.21 shows the location of the target, and Figure 6.22 shows the location of the camera.

Figure 6.21 Sensors and target on the pier

Figure 6.22 Camera setup

6.3.2 Data Processing

Figure 6.23 shows the raw data from accelerometers in actual physical units for the train crossing. The DC offset in the signals was due to the signal conditioner settings. This offset was removed during the data processing.

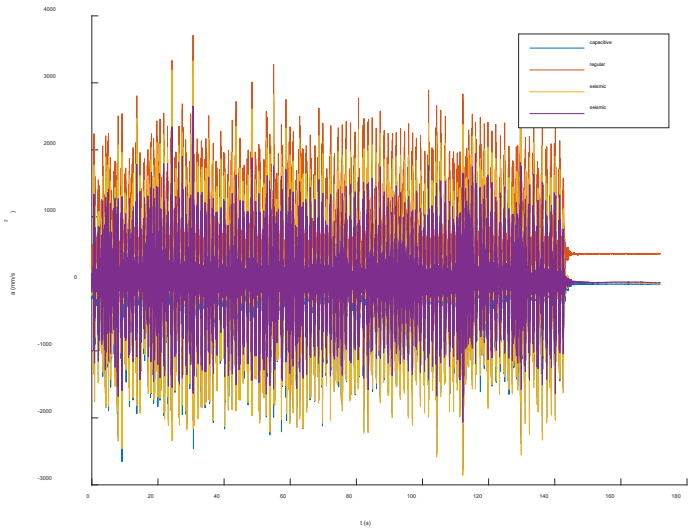

Figure 6.23 Raw accelerations in vertical direction for pier cap

Most of the important frequency content of the measured signal was in the low frequencies. Figure 6.24 shows the PSD of the accelerations for the low frequencies only. Note the generally good agreement between the PSDs.

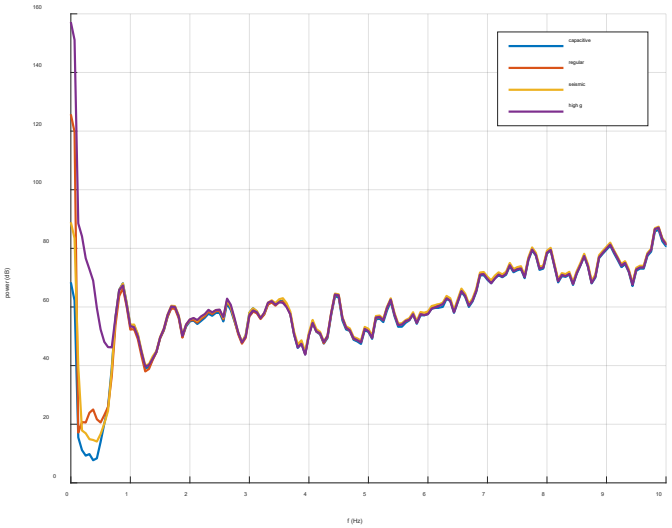

Figure 6.24 PSD for the pier cap

6.3.3 Results Comparison

To assess the adequacy of the data, the PSD of the displacement signal was obtained. In addition, the researchers obtained the PSD of the estimated displacement signal using FDE. Figure 6.25 shows the results for both piers. Consistent data should have agreed well for frequencies larger the target frequency.

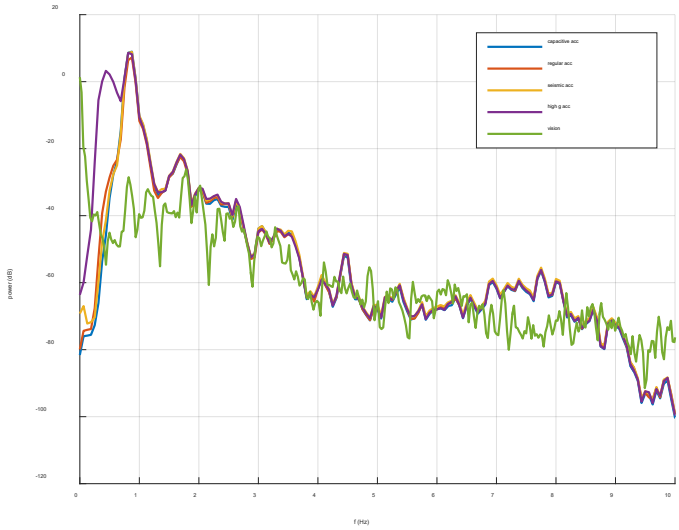

Figure 6.25 PSD of vertical displacements of the pier cap

In the vertical direction, the displacement PSD results matched reasonably well for low frequencies. Note that for the vertical displacement, the important frequency content is located in the lower frequencies, which means that most of the displacement was pseudo-static.

The researchers extracted dynamic displacement from the vision data using traditional high-pass Butterworth filters, as before.

Finally, researchers applied the reference-free algorithm to the accelerations with parameters explained in Section 4. Figure 6.26 shows the results for the pier cap, which matched well with the vision results. Note that vertical displacements were not that important for timber trestle bridges, since the response consisted mainly in axial vibration of the piles, which typically have large frequencies.

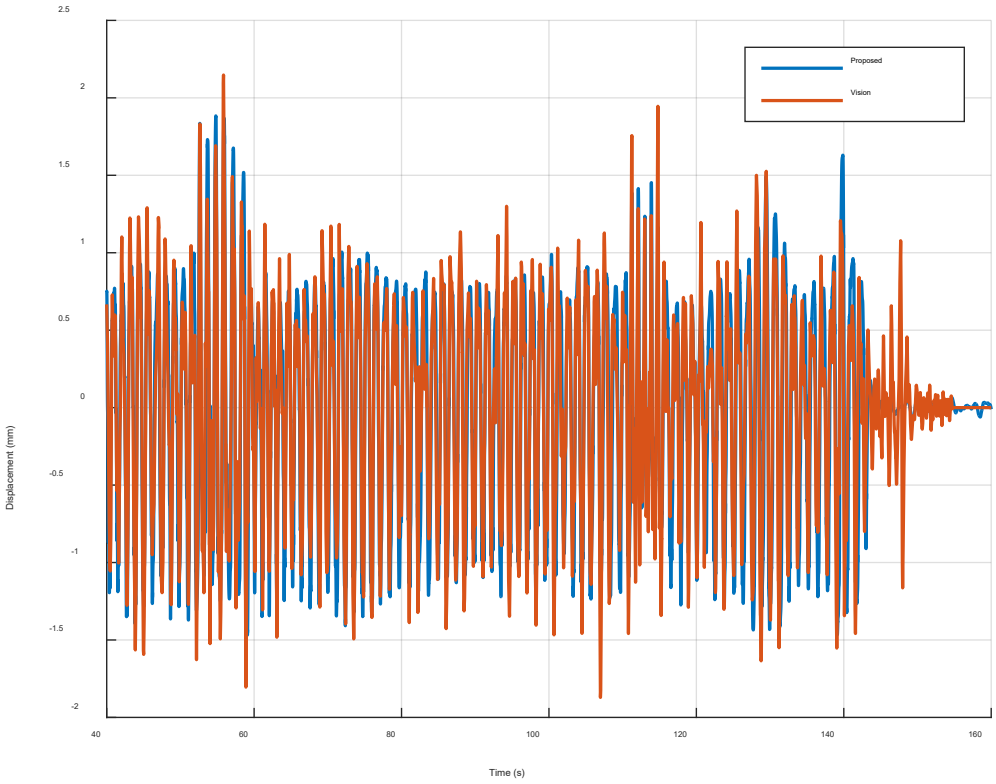

Figure 6.26 Dynamic vertical displacement comparison for pier cap

These results demonstrate the efficacy of the proposed approach. The estimated lateral displacements for the Freeport 78.0 and 78.3 bridges matched well when compared with the vision-based displacement measurements, as did the estimated vertical displacement for the Freeport 33.00 bridge.

7. Conclusion

This research project has developed a cost-effective and practical reference-free method to estimate displacement from measured accelerations. The method was validated via numerical simulations, laboratory testing, and full-scale field tests. The following sections summarize the results of this project and provide a gap analysis to guide future research.

7.1 Identified Industry Concerns

Current FRA limits for track alignment are much larger than measured transverse displacements for timber or steel railroad bridges found in the literature. In addition, misalignments may exist in bridges that are not reflected on tracks until repair is no longer an option. The existing limits are only for design purposes, and current practitioners recognize and agree that these limits are too liberal for evaluating the health of existing bridges. Moreover, there are no AREMA limits for transverse displacement in timber bridges.

Industry experts' biggest concerns are: timber pile displacements in all directions, timber beam displacements in the vertical direction, steel beam displacements in all directions, steel crack width on floor beams, pin-connected trusses' eye-bar vibrations, permanent settlement over time in large piers, and scouring over time for all types of bridges

No set metrics or limits are available regarding the in-service displacement of bridges. Guidance is available only for design limits. Railroads and researchers have a general interest in collecting more displacements in the field, which can inform what those limits should be to prioritize bridge replacements, but are limited by the cost and difficulty of current methods to measure displacements.

7.2 Development and Validation of a Reference-free Method for Collecting Bridge Displacements

Displacement responses from a structure can be obtained by direct contact type, non-contact type, and reference-free methods. LVDT is representative of the type of sensors employed in contact type measurements. This method requires a connection between the structure and the ground, and installation is difficult. Non-contact methods can measure the displacement of a structure from a remote location, for instance a LDV or vision-based system. However, measurement accuracy depends on the device mounting condition on a reference point. A reference-free method uses other types of measurements, such as acceleration and strain. Researchers commonly use accelerometers in the dynamic testing of structures due to installation convenience and relatively low cost and noise. Indirect estimation using acceleration responses has the potential to be widely adopted for obtaining structure displacement information.

To recover displacements from accelerations, previous researchers have considered the minimization problem with regularization, and then they solved it by finite difference or frequency-domain methods. The research team studied the previous approaches and developed a new method based on an FIR filter, which is stable and can be applied directly in the time-domain. The researchers performed a parametric analysis to determine the optimum parameters of the filter. In addition, they developed a technique to compute efficiently the coefficients of the FIR filter, which is especially suitable for WSS implementation.

To illustrate the accuracy of the method, the researchers performed numerical analyses on field data from Bluford, Illinois bridge, and compared the results with a previous method. The previous approach showed a large RMS error variance, from 3.52 percent to 18.21 percent, in and a 4.10 percent to 25.63 percent peak-to-peak error. The proposed method has a maximum error of 3.55 percent. Furthermore, researchers reproduced the Bluford, Illinois bridge field data in the hydraulic motion simulator, from which they measured displacements and accelerations. The experimental validation indicated that the proposed displacement estimation method estimates dynamic displacement very well; the maximum error was 3.59 percent. The maximum error of the experimental validation was comparable to the numerical validation.

7.3 Applied Camera-based Methods to Estimate Displacements

Instead of using LVDT to measure displacements, researchers used a computer-vision-based approach to measure the displacement of the bridge as a reference. The proposed method approach is composed of camera calibration, natural feature detection, and feature tracking.

To confirm the accuracy of the vision-based methods, researchers built a FE model of the bridge under train loading to estimate vertical displacements. The model considered train loads as concentrated moving loads, and it included the additional mass of the train as concentrated moving masses. Researchers used Simulink to solve the first-order system in time for the train loading. The agreement in shape and magnitude are formidable, which means that the results from the vision-based method were reliable.

7.4 Validated Displacements Estimations On Timber Trestle and Pin-connected Steel Truss Bridges

The researchers monitored three bridges: two timber trestles and one pin-connected steel truss, to measure displacements and accelerations. They applied the proposed algorithm to the accelerations in the lateral directions for the Freeport 78.00 bridge. The results matched well for both magnitude and phase. The peak-to-peak error was less than 1 percent, and the RMS error was approximately 1.6 percent. The results from pier 6 and pier 7 matched well up to a phase delay due to their spatial location.

The researchers applied the proposed algorithm to the accelerations in the lateral directions for the Freeport 78.30 bridge. Again, the results matched well for both magnitude and phase. The peak-to-peak error was less than 3 percent, and the RMS error was approximately 2.1 percent.

Because of problems in the measured data in the vertical direction for the previous field tests, campaign monitoring was conducted for the Freeport 33.00 bridge. This bridge was selected because of convenient access. Researchers applied the proposed algorithm to the measured accelerations in the vertical direction. The results matched well.

7.5 Gap Analysis

This section identifies technological gaps that new research should address. Research that fills these gaps will achieve the full potential of this technology for managing railroad bridge infrastructure.

- **Develop an efficient implementation of the algorithm in the new generation of WSS.**

Gap #1: The Imote2 is no longer available. Porting the algorithm to a new generation of WSS, such as the Xnode, is required.

- **Develop graphical user interface GUI for efficient decision making.**

  Gap #2: The data collected requires interpretation; hence, the researchers need to develop a graphical user interface to visualize the data in near-real time.

  Gap #3: The system should include an automatic bridge classification from collected data, and compare the bridge performance with safety thresholds to expedite decision-making.

- **Campaign monitoring of railroad bridge in different conditions**

  Gap #4: Despite the good results presented in this research project, monitoring of more bridges is still required to develop a database of experience. A larger number of bridges should be monitored. For example, 10 timber trestle bridges and 10 pin-connected steel truss bridges in different conditions should be monitored to obtain service displacements using the Xnode with the algorithm embedded as described in Gap #1.

- **Develop displacement limits to have a reference of comparison to estimate bridge performance.**

  Gap #5: Despite developing a reliable algorithm for displacement estimation, displacement limits for different bridge conditions are not available. Additional bridge monitoring is required to develop adequate displacement performance limits, which is now possible using WSS and the reference-free analysis method.

In summary, the results of this project provide a strong foundation for the development of simplified and effective campaign monitoring of railroad bridges using new-generation WSS, the Xnode. Gap analysis demonstrated that expanding this project will enhance the applicability of the developed methodologies to different classes of the railroad bridges. The next section details further research needed to fulfill the vision and realize the benefits of using WSS for North American railroads.

8. Recommendations for Continued Research

Freight transportation in North America is widely considered the best in the world, with 40 percent of the nation's freight tonnage carried by railroads.[26] Because many parts of the current railroad networks are over 100 years old, railroads in North America have doubled capital investments in the last few decades. Therefore, they must determine bridge performance and safety thresholds (e.g., green, yellow, and red) that can assist them in managing/maintaining bridge assets and prioritizing repairs.

Lateral and vertical displacements of bridges under trainloads are widely believed to provide a good measure of the condition of a bridge.[2,10] However, as discussed in Section 1.1, two significant problems have hindered the use of displacements in bridge condition assessment:

1) The scarcity of displacements measurements of railroad bridges to date has been due, in part, to the high cost of instrumenting a railroad bridge to measure displacements under revenue service traffic. In many circumstances, installing a reference near the bridge from where to measure is not even possible. Therefore, the collection of displacements in railroad bridges is limited currently to infrequent situations.
2) The industry has not established standards for acceptable displacement limits. Once collected, a critical issue in using displacements to assess bridge condition is determining the meaning of these displacements in the context of railroad bridge safety under revenue service traffic. Current limits regarding displacements are oriented toward design; new limits need to be developed that relate better to the different levels of service expected for railroad bridges during their life.

This research has addressed the first problem – developing a reference-free method for displacement estimation for use with WSS. The developed approach has been validated in the laboratory and the field. More research to solve the second problem is required.

8.1 Recommendations

Based on the outcomes of this research effort, the gap analysis in Section 7.2, and the vision of the future stated previously, the Illinois research team recommends the following tasks be carried out to realize of the full potential of wireless sensor technology in managing railroad bridge infrastructure:

Task # 1: Port Algorithms to the Xnode (Gap #1)

This task consists in porting the reference-free displacement estimation algorithm developed under current FRA funding to the Xnode, since the Imote2 WSS is no longer available. The Xnode is a next-generation wireless sensor node developed at UIUC specifically designed to meet the demands of railroad monitoring applications. Porting software to the new wireless sensor node will enable the automatic estimation of the displacements from the obtained accelerations. The ported algorithm should be validated in the laboratory by mounting the Xnode on a hydraulic simulator and playing back previously measured bridge displacements.

[26] GeoMetrx. (2013, December 22) High Speed Rail: A Vision for the Future. geometrx.com.

Task # 2: Develop GUI for Efficient Decision Making (Gap #2, 3)

The second task is to develop a graphical user interface (GUI) that will allow collected data to be visualized in near-real time. This task should also include prototyping a method to automatically classify bridge condition based on measured displacement using machine learning methods. Finally, decisions can be facilitated by comparing the estimated data with bridge performance and safety thresholds (e.g., green, yellow, and red) as well as previous inspection reports.

Task # 3: Campaign Monitoring of In-service Railroad Bridges (Gap #4)

Working closely with industry partners, a total of 20 bridges (10 timber trestle and 10 pin-connected truss bridges) with varying conditions should be selected. Researchers should deploy the Xnode on these bridges and use the developed approach to determine displacements under revenue service train loads. Bridges should come from the bridge replacement program in order to be of interest to the industry partners. In addition, a computer-vision-based approach could be used to measure the displacement and be compared with the proposed method for validation purposes.

Task # 4: Develop Bridge Performance Thresholds (Gap #5)

After data collection, the results should be put in a database and used to develop bridge performance and safety thresholds (e.g., green, yellow, and red), mentioned in Task # 2. The primary focus should be relating the estimated displacement for each class of bridge (e.g., timber trestle or steel truss) with specified conditions. Relating displacement magnitudes with existing bridge conditions will allow a better basis for both maintenance/repair/replacement and safety decisions.

Task # 5: Documentation and Technology Transfer

A comprehensive report documenting the results of Tasks 1–4 should be included in a final report to FRA. Additionally, the results should be presented at the annual AREMA meeting to inform the community about these developments.

Abbreviations and Acronyms

AREA	American Railway Engineering Association
AREMA	American Railway Engineering and Maintenance-of-Way Association
BAA	Broad Agency Announcement
CN	Canadian National
FDE	Fast Displacement Estimation
FRA	Federal Railroad Administration
FRF	Frequency Response Function
HSR	High-Speed Rail
IC	Illinois Central
LVDT	Linear Variable Differential Transformer
NB	Northbound
PSD	Power Spectral Density
RailTEC	Rail Transportation and Engineering Center
RMS	Root Mean Square
SB	Southbound
SSTL	Smart Structures Technology Laboratory
USDOT	U.S. Department of Transportation
WSS	Wireless Smart Sensor